The concept of direct adaptive control for improving voltage and frequency regulation loops in several power system applications

Abubakr, Hussein; Vasquez, Juan C.; Hassan Mohamed, Tarek; Guerrero, Josep M.

Published in:
International Journal of Electrical Power and Energy Systems

DOI (link to publication from Publisher):
10.1016/j.ijepes.2022.108068

Publication date:
2022

Document Version
Publisher's PDF, also known as Version of record

Electrical Power and Energy Systems 140 (2022) 108068

Contents lists available at ScienceDirect

International Journal of Electrical Power and Energy Systems

journal homepage: www.elsevier.com/locate/ijepes

The concept of direct adaptive control for improving voltage and frequency regulation loops in several power system applications

Hussein Abubakr [a,b,*], Juan C. Vasquez [a], Tarek Hassan Mohamed [b], Josep M. Guerrero [a]

[a] Center for Research on Microgrids (CROM), AAU Energy, Aalborg University, 9220 Aalborg, Denmark
[b] Department of Electrical Engineering, Faculty of Energy Engineering, Aswan University, Aswan 81528, Egypt

ARTICLE INFO

Keywords:
Adaptive control
Egyptian power system
Automatic voltage regulator
Power system stabilizer
Harris hawks optimizer
Excitation system
Three-area interconnected microgrid
solar PV farm

ABSTRACT

This article presents the idea of direct adaptive control for several power system applications such as the Egyptian power system (EPS), a three-zone interconnected microgrid (MG), and a single machine connected to the grid (SMIB). The main concept of the proposed adaptive method is built on the tuning of the controller gains using Harris hawks optimizer (HHO). In order to maintain the frequency and voltage at their nominal values, a modified virtual rotor (virtual inertia + virtual damping) is investigated as a tertiary control loop within the proposed EPS and the 3-area MG system. For SMIB application, a secondary automatic voltage regulator (AVR) has been added to the primary AVR within the excitation system to offer more adequate damping characteristics for the synchronous generator of the studied system. Where the proportional-integral-derivative power system stabilizer (PID-PSS) is connected to the excitation system for a single machine tied to the grid to significantly mitigate low-frequency oscillations due to various expected faults and undesirable operating conditions. The proposed direct adaptive control strategy has been used to tune the integral controller of the secondary AVR and PID for SMIB application, and also to adjust the virtual rotor in the EPS and the 3-area MG applications. The operative performance of the introduced adaptive secondary AVR is assessed against the conventional system (no PSS), Lead-Lag PSS, and PSS type 2 based PSO and WECC standard under the effect of a 3-φ short-circuit fault subjected at the grid bus considering solar photovoltaic (PV) farm-based grid. Moreover, the EPS system and 3-area MG are evaluated under the effect of load change conditions and partial injection of PV and random loads. The final findings prove that the direct adaptive concept can provide robust performance and effectively maintain the dynamic stability of the main grid against fluctuations.

1. Introduction

In modern power grids, frequency stability is one of the significant problems related to large-scale power systems. High-frequency oscillations occur when the unbalanced power is not compensated by the load frequency control system (LFC). Therefore, these systems are becoming more complex due to identical or mismatched uncertainties, load variations, and time delays [1,2].

Over the past decades, the PID controller has acted as the main player to control the practical and industrial processes. It has several benefits when used in the LFC to maintain the power in tie-line and regulate the frequency according to schedule value: simplicity, reliability, and low cost [3,4]. In addition, it has the disadvantage of being less sensitive to process parameter changes and system disturbance [5]. Therefore, several robust, intelligent, optimal, and adaptive control approaches have been explained in [6-11]. In this study, the concept of direct adaptive control technique was applied to tune the modified virtual rotor parameters (inertia + damping) and adjust the integral control gain of the secondary automatic voltage regulator (AVR).

With the growing share of renewable energy generation sources (RESs), it raises new stability issues in the regulation of large/micro grids. A major problem is the reduction of inertia and damping in the system due to the replacement of conventional generations (i.e., synchronous generators SGs) with RESs [3,12]. The main reason for lacking system inertia is the converters/inverters commonly used to deliver the RESs to the micro/large grids. These devices do not possess and retain any inertia or damping properties, resulting in degradation of system inertia and damping, larger frequency slip, instability, and collapse of the system. To address stability issues, a new inertial control scheme called virtual synchronous generator (VSG) [13-15] was designed to emulate virtual inertia power based on the dynamic behavior of SGs and

* Corresponding author at: Center for Research on Microgrids (CROM), AAU Energy, Aalborg University, 9220 Aalborg, Denmark.
E-mail address: haha@energy.aau.dk (H. Abubakr).

https://doi.org/10.1016/j.ijepes.2022.108068
Received 7 November 2021; Received in revised form 12 January 2022; Accepted 13 February 2022
Available online 9 March 2022

Nomenclature

Δf	EPS frequency deviations (Hz)
ΔP_m	Changes in mechanical power (MW pu)
ΔP_L	Changes in EPS random loads (MW pu)
ΔP_c	Supplementary control
ΔP_{PV}	Solar power variations
ΔP_{tie}	Change in tie-line power (MW pu)
$\Delta P_{Inertia}$	Changes in virtual inertia active power
$\Delta\omega_r$	Rotor speed deviation (rad/s pu)
D_{EPS}	System damping coefficient of the EPS (pu MW/Hz)
H_{EPS}	Equivalent inertia constant (pu sec)
R_1	Governor speed regulation non-reheat plant (Hz/pu MW)
R_2	Governor speed regulation reheat plant (Hz/pu MW)
R_3	Governor speed regulation hydro plant (Hz/pu MW)
m	The fraction of turbine power
P_{n1}	Nominal rated Power output for the non-reheat plant (MW pu)
P_{n2}	Nominal rated Power output for the reheat plant (MW pu)
P_{n3}	Nominal rated Power output for the hydro plant (MW pu)
T_1	Valve time constant of the non-reheat plant (s)
T_2	Steam valve time constant of reheat plant (s)
T_3	Water valve time constant hydro plant (s)
T_d	Dashpot time constant of hydro plant speed governor (s)
T_h	The time constant of reheat thermal plant (s)
T_w	Water starting time in hydro intake (s)
T_{ESS}	Inverter-based ESS time constant (s)
T_{PV}	Solar system time constant (s)
T_{ij}	Tie-line synchronizing coefficient between subareas i th and j th
T_e	Electrical torque
T_m	Mechanical torque
I_{PV}	Solar PV farm current in (A)
V_{PV}	Solar PV farm voltage in (V)
V_t	Synchronous machine terminal voltage in (V pu)
P_M	Hydro turbine mechanical power in (MW pu)
$G_{OLTF}(s)$	The open-loop transfer function without droop characteristics
$G_{CLTF}(s)$	The closed-loop transfer function with droop characteristics
J_{VI}	Virtual inertia constant
D_{VI}	Virtual damping constant
ω	Rotor speed (rad/s)
J	Moment of inertia (kg m^2)
K_{PSS}	Stabilizer gain
K_P	Proportional controller gain
K_i	Integral controller gain
K_D	Derivative controller gain
K_{ir}	The integral AVR gain
K_A	Regulator gain of excitation system
K_E	Exciter gain
K_f	Damping filter gain
T_{TEM}	Time constant of the controller in (s)
T_A	Regulator time constant in (s)
T_E	Exciter time constant in (s)
T_f	Time constant of damping filter in (s)
T_{wo}	Signal wash out time constant (s)
$T_{1o}-T_{4o}$	Lead-Lag time constants (s)
βi	Frequency Bias
ω_n	Natural frequency
ζ	Damping ratio
M_P	Maximum overshoot
T_s	Settling time in (s)
J_{min}	Objective function
H	Nominal system inertia (MJ/MVA)
$E_{kinetic}$	Kinetic energy stored in the system

Acronyms

MG	Microgrid
SG	Synchronous generator
HTG	Hydro turbine generator
HHO	Harris hawks optimization
AVR	Automatic voltage regulator
EPS	Egyptian power system
PSS	Power system stabilizer

improve system performance and stability.

The concept of the VSG is initially relying on replicating the dynamical properties of a real SG of power electronics-based DG/ RES units, in order to inherit the stability-enhancing merits of an SG [3]. The mechanism of the virtual rotor is constructed by the inverter, short-term energy storage system (ESS), and appropriate control technique. Given the limited cost of batteries that make the VSG configuration more difficult to control using only batteries, we are considering adding a portion of the VSG control signals to the LFC signal used for non-reheat, reheating thermal, hydropower plants (the suggested EPS system).

This paper proposes a modified design and analysis of virtual rotor based on the derivative technique to simultaneously imitate damping and inertia properties in the EPS system, thus enhancing frequency stability and durability under a wide range of system operations. Proposed studies have shown that the modified virtual rotor can be performed in such a way that provides virtual inertia and virtual damping capability into the EPS.

Another application to support our proposed method is to use a single machine connected to the grid. SG is a vital element of each power system. It is largely controlled by the excitation system [16], which is used to maintain the system stable because it has a faster AVR to get rid of the synchronous torque with a small effect on damping. This can be achieved using the power system stabilizer (PSS) output signal and introducing it into the exciter system as discussed below in Section 7.

The PSS provides a complementary signal to the excitation system to enhance oscillating instability more quickly. At present, PSS and AVR are widely utilized in several applications to achieve some international standard [17,19]. In [18], a strategy based on deep reinforcement learning (DRL) is proposed as an intelligent coordinator for PSS and AVR in multi-area power grids. With the expansion of the power electronic technology, a flexible excitation system with fully controlled devices is introduced in [20,21]. Not only can power be supplied to the field winding but also injection reactive power to the generator terminal. Compared to the conventional AVR and PSS controlled excitation voltage system [21], it contains two damping channels to provide a more stable and flexible control potential.

The proposed applications (AVR) and (LFC) represent key challenges to support the operation, control, and security of power systems [22]. AVR is employed to diminish the losses in active-reactive power and generate a stable tracking process for reference voltage. Deviations in the operating voltage levels greatly affect the stability of power system units. On another side, LFC is needed to regulate the deviations in frequency caused by dynamic active load changes and prevent oscillations from expanding into a multi-area grid [3,8].

Recently, the control parameters have been tuned optimally using optimization techniques because of their ability to respond to suspicions and disturbances [23-25]. They have been used to make offline and online tuning of LFC parameters in an adaptive manner [3 5,26-28].

In this work, a metaheuristics optimization technique called 'Harris hawks optimizer (HHO)' [29] was proposed for calculating the optimal value of the secondary AVR' integral controller gain, virtual inertial and virtual damping parameters according to system dynamics. One of the advantages of HHO is the requirement of fewer insensitive users. Additionally, HHO can be applied in a wide range of optimization issues due to its plain of use, high-speed convergence, less computational time to report the optimal solution.

The main contribution of this work can be outlined as follows:

- The concept of direct adaptive control has been employed in three applications: the Egyptian power system, a three-area interconnected MG, and the single machine connected to the grid.
- A modified virtual rotor (inertia + damping) has been suggested for EPS and 3-area MG frequency regulation.
- A new secondary automatic voltage regulator (AVR) has been added to the excitation system to generate a stable tracking process for reference voltage.
- The parameters of virtual inertia, virtual damping, PID gains of PSS and integral controller gain of secondary AVR are adaptively tuned using the HHO optimizer.
- The proposed control strategy can efficiently deal with system difficulties such as 3-φ short-circuit fault, load variations, and partial and full injection of solar PV farm, and random loads.

1.1. Work Motivation

Conventional controllers are designed by considering fixed parameters, but the system keeps showing rogacity to a certain extent. However, if the parameter values change somewhat, abnormal behavior may happen resulting in instability and collapse of the system. Therefore, an appropriate strategy to control is mandatory to help in stabilizing the system, in addition, providing a high capability for rejecting the turbulence over a wide parameter variations range. For this intent, design a robust control is needed to withstand adverse operating conditions. Recently, the concept of adaptive control has demonstrated its ability to deal with parameters changes and uncertainties. Adaptive control categorized into two types: Direct (this type is proposed in this study) and the second is indirect approach involves a shifting variable that is modified to enhance the system performance and robustness at the desired sensitivity. The efficient performance and plain computation of the direct adaptive control approach have prompted and led us to study its implementation with regard to LFCs issues and Excitation systems.

2. System under study

2.1. First application: Egyptian power system

The Egyptian power system (EPS) includes many traditional sources of generation (i.e., thermal, gas, and hydraulic power plants), and RESs (i.e., PV and wind turbines). These plants are classified into 3 categories; (a) Non-reheat, (b) Reheat, and (c) Hydraulic power plants [30]. The overall installed capacity for EPS is 58. 5 GW with the peak load is 32.4 GW stated by the end of 2019 [31], and the installed capacity consists mainly of combined-cycle plants (55.7%). Moreover, the share of RESs today, including wind turbines and PVs, only represents 3.8% of overall capacity. Therefore, Egypt aims to increase the sharing power from RESs to 20% by 2022, and 42% by 2035 [31,32]. The dynamic EPS model considering RESs, conventional plants, and VSG is shown in Fig. 1.

The simplified EPS model with the proposed coordination scheme is shown in Fig. 2, and the nominal EPS system with modified virtual rotor parameters is given in Table 1 [30,33]. The parameters of PID gains were calculated in the EPS model using HHO considering the penetration of RESs.

In this paper, simulated PV and random loads power are presented. The solar PV plant is modeled as a 1st order transfer function of a unity gain as shown in Fig. 1 with a rated power of 5 GW (in accordance with Egypt's 2035 target including Benban PV plant and other future projects). In addition, the validity of EPS using random loads of 15 GW power with a base power of 59.5 GW (full EPS capacity) was verified, and finally, 5 MW of ESSs were installed in the EPS.

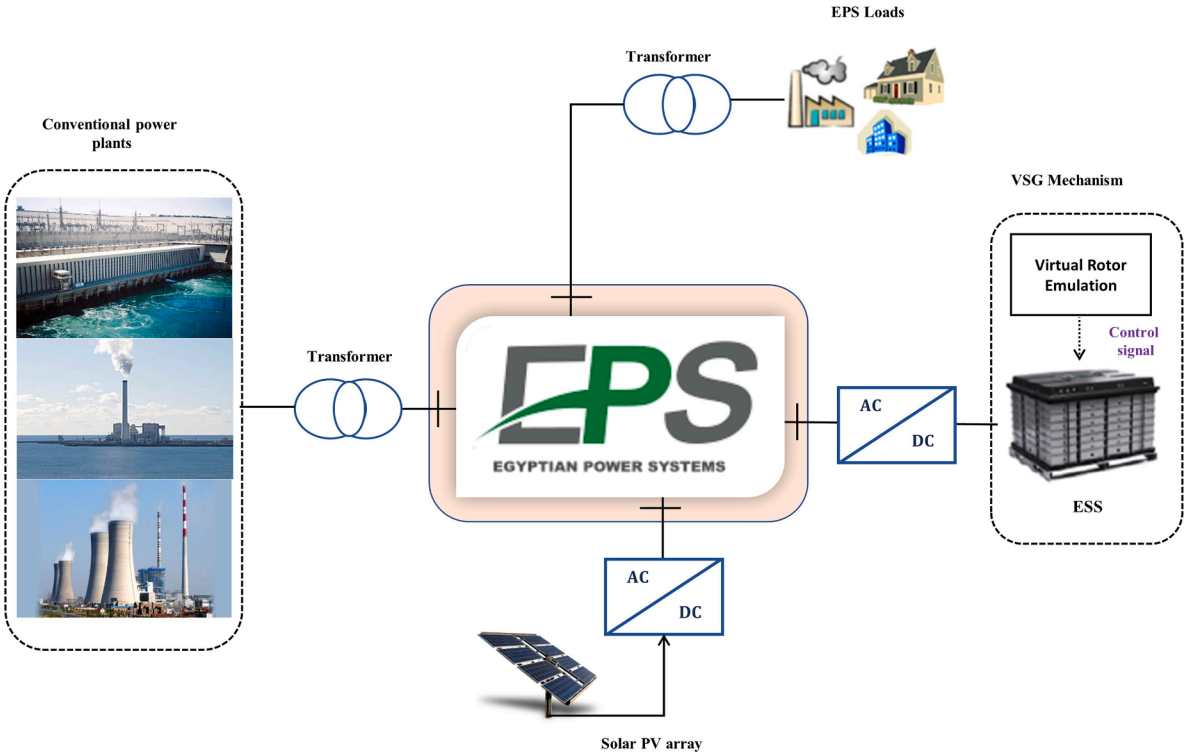

Fig. 1. A dynamic model of the EPS considering RESs within the presence of a virtual inertia mechanism.

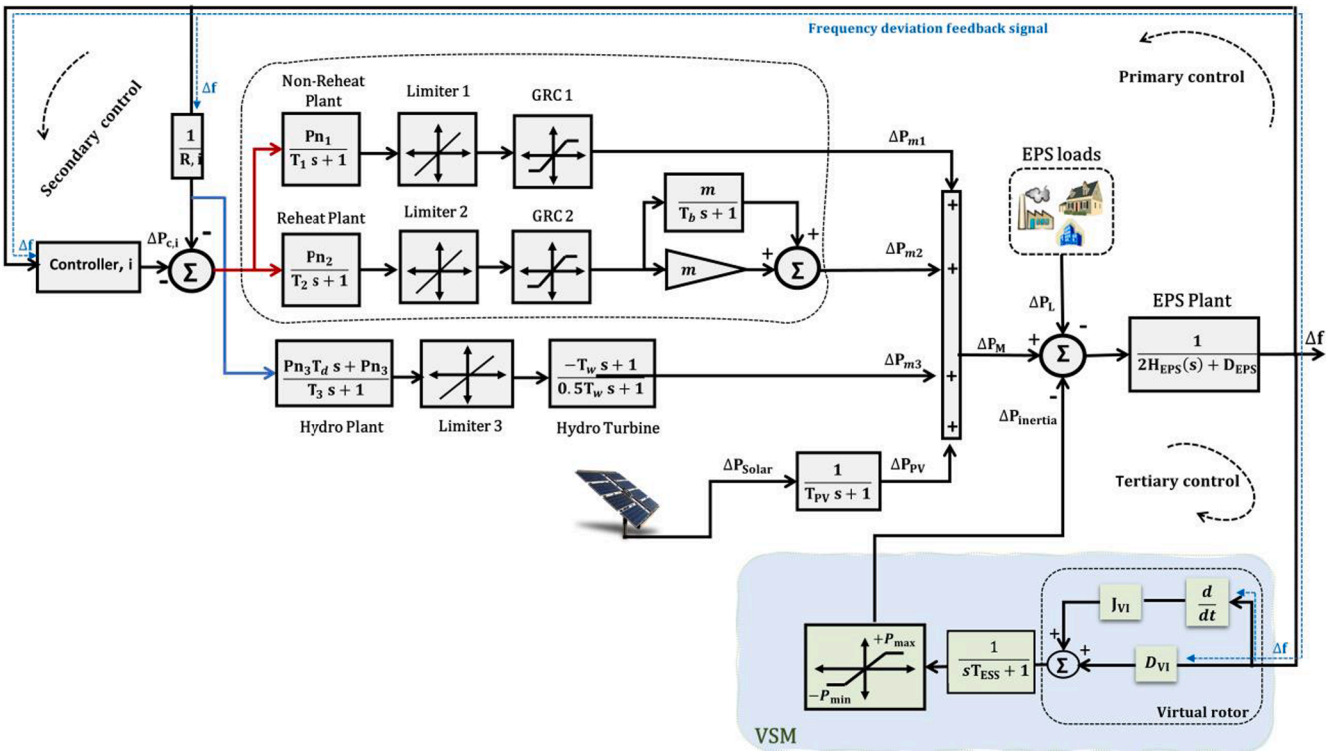

Fig. 2. A simplified model of the EPS supported with a modified virtual rotor mechanism.

Table 1
Initial Parameters of EPS Grid.

Parameter	Value	Parameter	Value
D_{EPS}	0.028	P_{n2}	0.6107
H_{EPS}	5.7096	P_{n3}	0.1364
R_1	2.5	T_1	0.4
R_2	2.5	T_2	0.4
R_3	1.0	T_3	90
m	0.5	T_d	5.0
K_P	26.5370	T_h	6.0
K_I	16.3125	T_w	1.0
K_D	−0.508	T_{PV}	10
P_{max}	0.2	T_{ESS}	10
P_{min}	−0.2	J_{VI}	Adaptively tuned
P_{n1}	0.2529	D_{VI}	Adaptively tuned

The frequency deviation (Δf) of the studied EPS can be obtained looking at the effect of the primary (droop), the secondary control loop (LFC), and tertiary modified virtual rotor control loop (inertia + damping) as follows [33]:

$$\Delta f = \frac{1}{2Hs + D}(\Delta P_M - \Delta P_L \pm \Delta P_{Inertia}) \quad (1)$$

$$\Delta P_M = \Delta P_{m1} + \Delta P_{m2} + \Delta P_{m3} + \Delta P_{PV} \quad (2)$$

$$\Delta P_{m1} = \frac{P_{n1}}{T_1 s + 1} * \left(\frac{-1}{R_1} * \Delta f - \Delta P_c\right) \quad (3)$$

$$\Delta P_{m2} = \left(m + \frac{m}{T_h s + 1}\right) * \frac{P_{n2}}{T_2 s + 1} * \left(\frac{-1}{R_2} * \Delta f - \Delta P_c\right) \quad (4)$$

$$\Delta P_{m3} = \left(\frac{-T_w s + 1}{0.5 * T_w s + 1}\right) * \frac{P_{n3} T_d s + P_{n3}}{T_3 s + 1} * \left(\frac{-1}{R_3} * \Delta f\right) \quad (5)$$

$$\Delta P_{PV} = \left(\frac{1}{T_{PV} s + 1}\right) * \Delta P_{Solar} \quad (6)$$

$$\Delta P_{inertia} = \frac{J_{VI} s + D_{VI}}{1 + s T_{ESS}} (\Delta f) \quad (7)$$

where $\Delta P_{m,i}, \Delta P_L, \Delta P_{Inertia}, \Delta P_{PV}, and \Delta P_c$ mean changes in the mechanical, load, inertia, solar, supplementary control power, respectively.R is the governor speed regulation and m is the fraction of turbine power. T_h is the time constant of reheat thermal plant,T_w is the dashpot time constant of hydro plant, and water, and T_d is the water starting time of the hydro plant. P_{n1}, P_{n2}, P_{n3} are the normal output rated power of non-reheat, reheat, hydropower plants, respectively.J_{VI} means the virtual inertia constant. D_{VI} means the virtual inertia damping constant. T_{ESS} is the inverter-based ESS time constant.

3. Virtual rotor emulation technique (inertia and damping)

In old communities or power systems, the kinetic energy (initial inertia) stored in the system rotating mass with spinning loads is defined as [33,34]:

$$E_{kinetic} = \frac{1}{2} J \omega^2 \quad (8)$$

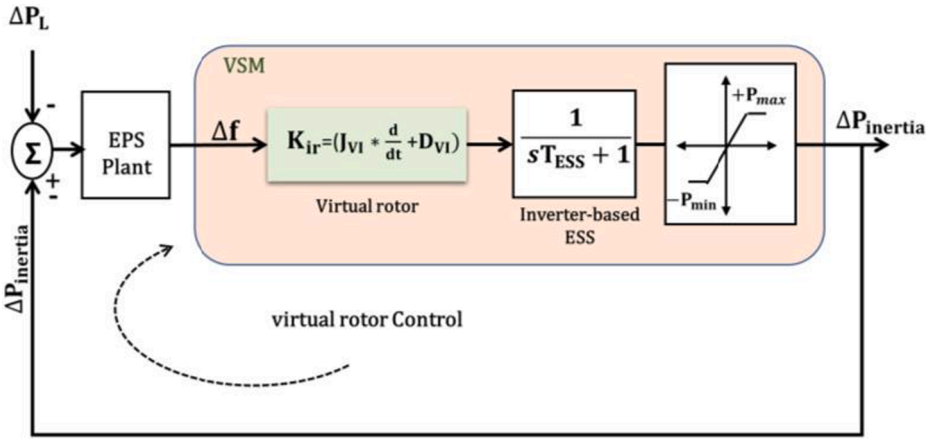

Fig. 3. The dynamic structure of the modified virtual inertia emulation based ESS connected to EPS.

where ω stands for rotor speed (rad/s) and J indicates the system's moment of inertia (kg.m^2). By given the change rate of rotor speed, it relates to balance in torque of spinning mass defined as:

$$T_m - T_e = \frac{P_m}{\omega} - \frac{P_e}{\omega} = J^* \frac{d\omega}{dt} \tag{9}$$

where P_m means the mechanical power and P_e is the electrical power. T_m and T_e mean the mechanical torque and electrical torque, respectively.Thus, the stored kinetic energy $E_{kinetic}$ can be calculated as proportional to the rate of power. It is called the system inertia as:

$$H = \frac{E_{kinetic}}{s} \tag{10}$$

where H is the inertia of the system, S is the system rated apparent power in (VA). Accordingly, the rate of change of frequency (ROCOF), which is used to evaluate the system inertia is calculated as follows:

$$\frac{d\omega}{dt} = \frac{\omega^2(T_m - T_e)}{2Hs} = \frac{\omega(P_m - P_e)}{2Hs} \tag{11}$$

Virtual inertia emulation is a new set of control techniques, ESSs, and power electronics that can virtually emulate an inertia power based on a conventional system (i.e., power system-based SG) into the power community-based RESs. Fig. 3 states the concept of emulation modified virtual rotor using an ESS-based derivative control method. The target is to compute the ROCOF using a derivative technique to add sufficient active power to the community [3,12]. Thus, the dynamic modified virtual rotor structure can mimic the desired inertia and damping characteristics of the community or power system, improving the overall inertia within the EPS system, frequency stability, and preventing power outages.

4. Indirect and direct adaptive control concept

For the indirect adaptive control method, it is applicable when the unknown parameters of a linear time-invariant plant lie in a known convex set throughout which no stable cancellation of the pole-zero occurs [35].

For our case study, Eq. (1) explains that the LFC is a turbulence rejection issue where the main objective is to design a controller for the EPS system to mimic the impact of load disturbance and parametric uncertainties. The open-loop transfer function without the droop characteristics:

$$G_{OLTF}(s) = G_{Gov,i}(s)G_{Turbine,i}(s)G_{EPS}(s) \tag{12}$$

Where (i = 1, 2, 3) according to plants type (non-reheat, reheat, and hydro) respectively as shown in Fig. 2.

The closed-loop transfer function for the EPS system:

$$G_{CLTF}(s) = \frac{G_{Gov,i}(s)G_{Turbine,i}(s)G_{EPS}(s)}{1 + \left(\frac{G_{Gov,i}(s)G_{Turbine,i}(s)G_{EPS}(s)}{R}\right)} = \frac{1}{a_3 s^3 + a_2 s^2 + a_1 s + a_1} \tag{13}$$

Where,

$$a_3 = (T_{Gov,i}T_{Turbine,i}) \times 2H_{EPS}$$

$$a_2 = 2H_{EPS} \times (T_{Gov,i} + T_{Turbine,i}) + (T_{Gov,i}T_{Turbine,i})$$

$$a_1 = 2H_{EPS} + T_{Gov,i} + T_{Turbine,i}$$

$$a_0 = D_{EPS} + 1/R_i$$

Previously, for simplicity, we convert Eq. (13) into a second-order system using the pad approximation procedure. This approach is based on the matching of Taylor series expansion coefficients about s = 0 (reference) [36]. Finally, the reduced-order is obtained as:

$$G_{reduced}(s) = \frac{-m_1(s) + m_0}{s^2 + n_1 s + n_0} \tag{14}$$

Therefore, there are many ways to minimize the order of the studied EPS system and convert it to second-order such as internal model control scheme IMC for reduction the model-order by neglecting some parameters to make the system act as second-order [37].

The main objective is to calculate the characteristic parameters such as damping ratio ζ and natural frequency ω_n so that we can control the maximum overshoot M_P and settling time T_s in an easy way. Indirect adaptive control methods have been done before in many kinds of research, so in this paper, we will only focus on direct adaptive control using soft techniques.

5. Overview of Harris hawks optimization

HHO was primarily introduced by Heidari et al. [29] The basic principle of the proposed HHO optimizer is based on hunting the prey by the hawks in some steps including tracing, encircling, closeness, and finally attacking. In this study, HHO is implemented as an adaptive

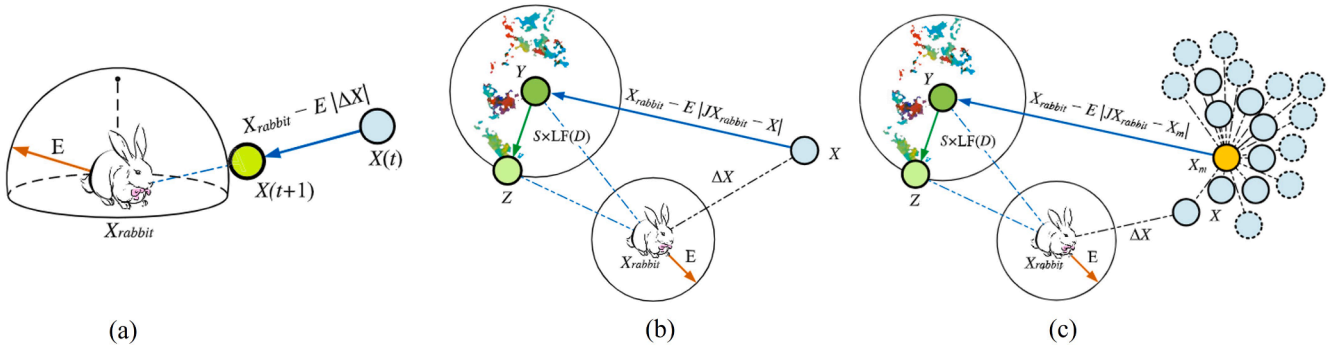

Fig. 4. Example of overall vectors in the case of (a) Hard besiege; (b) Soft besiege with progressive rapid dives; (c) Hard besiege with progressive rapid dives in 2D space [29].

controller as in [3]. It has many benefits such as plain coding, less computational time, and ease to use. In addition. It can be used to solve discrete, constrained, and unconstrained optimization issues. Therefore, the performance of this method is remarkable and powerful, unaffected by the wide dimension issue, so it is a robust metaheuristics optimizer.

The algorithmic details in the context of three stages are as follows:

a. Phase of Exploration
b. Phase of Transition from Exploration to Exploitation
c. Phase of Exploitation

A simple illustration for one hawk for all phases is demonstrated in Fig. 4 [29].

5.1. Performance assessment of HHO technique: Speed convergence test

In this sub-section, a statistical analysis for different benchmark test one objective functions is stated in Table 2. In addition, a comparative analysis to measure the performance and speed convergence of the proposed HHO compared to classical algorithms such as PSO (particle swarm), Jaya, ABC (artificial bee colony) and ESO (electro-search) optimizers was described in Table 2. The same number of populations and iterations have been used in each test function for resolving the optimization issues. A total of 20 independent running processes are performed for all algorithms, the best and worst values of these functions are constructed by taking 50 iterations and 50 as a size of population.

The validation of the optimizers depends on their speed convergence with optimum value. The optimal value of J_{min} is plotted against the number of J-evaluation in Fig. 5. It noted that the proposed optimizer converges relatively faster and gives superior to the other *meta*-heuristics and mathematical techniques in terms of the best and worst.

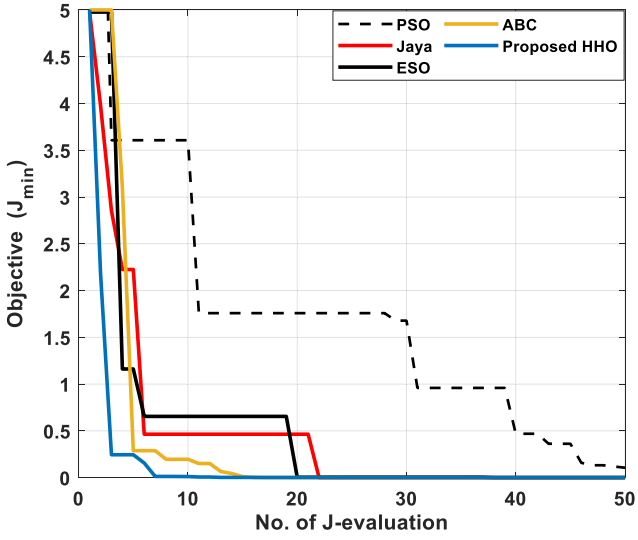

Fig. 5. Speed convergence characteristics of classic PSO, Jaya, ABC, ESO, and proposed HHO for a sphere function.

5.2. Adaptive virtual rotor based HHO

In order to achieve our objective function (J_{min}), a direct adaptive control theory is proposed using the HHO algorithm. This concept can help in determining the closed transfer function considering Δf as the main input of the modified virtual rotor along with the inverter-based ESS as shown in Fig. 3. The gain coefficients J_{VI} and D_{VI} are tuned using HHO optimizer relying on the Δf as an input to the optimizer. The desired J_{min} is a function of the on-time value of J_{VI} and D_{VI} and the nominal system $G(s)$.

For simplification, the dynamics of governor and turbine for reheat,

Table 2
Description of benchmark test functions and performance indexes.

Function name	Formula $f(x)$	D[a]	Search space	Statistic values	PSO	Jaya	ABC	ESO	HHO	f_{min}
Sphere	$\sum_{i=1}^{d}(x_i^2)$	5	[-5,5]	Best	1.79e^{-08}	4.77e^{-14}	1.68e^{-15}	1.01e^{-15}	1.78e^{-19}	0
				Worst	1.82e^{-08}	4.78e^{-14}	2.97e^{-16}	1.73e^{-14}	1.82e^{-18}	
Matyas	$0.26(x_1^2+x_2^2)-0.48x_1x_2$	5	[-5,5]	Best	1.52e^{-11}	4.22e^{-11}	1.48e^{-12}	7.09e^{-11}	2.36e^{-15}	0
				Worst	1.63e^{-11}	4.26e^{-11}	2.96e^{-09}	7.09e^{-09}	2.42e^{-15}	
Rastrigin	$-10d+\sum_{i=1}^{d}(x_i^2-10\cos(2\pi x_i))$	5	[-5,5]	Best	2.11e^{-09}	3.09e^{-09}	3.20e^{-015}	2.55e^{-013}	9.29e^{-18}	0
				Worst	1.94e^{-09}	3.22e^{-09}	3.21e^{-15}	2.42e^{-10}	9.33e^{-18}	
Ackley	$-20\exp\left(-0.2\sqrt{\frac{1}{d}\sum_{i=1}^{d}x_i^2}\right)-exp\left(\frac{1}{d}\sum_{i=1}^{d}\cos(2\pi x_i)\right)+20+\exp(1)$	5	[-5,5]	Best	3.85e^{-05}	2.70e^{-16}	2.72e^{-17}	2.38e^{-19}	1.56e^{-27}	0
				Worst	3.88e^{-05}	2.70e^{-16}	2.82e^{-16}	2.82e^{-19}	1.48 e^{-26}	

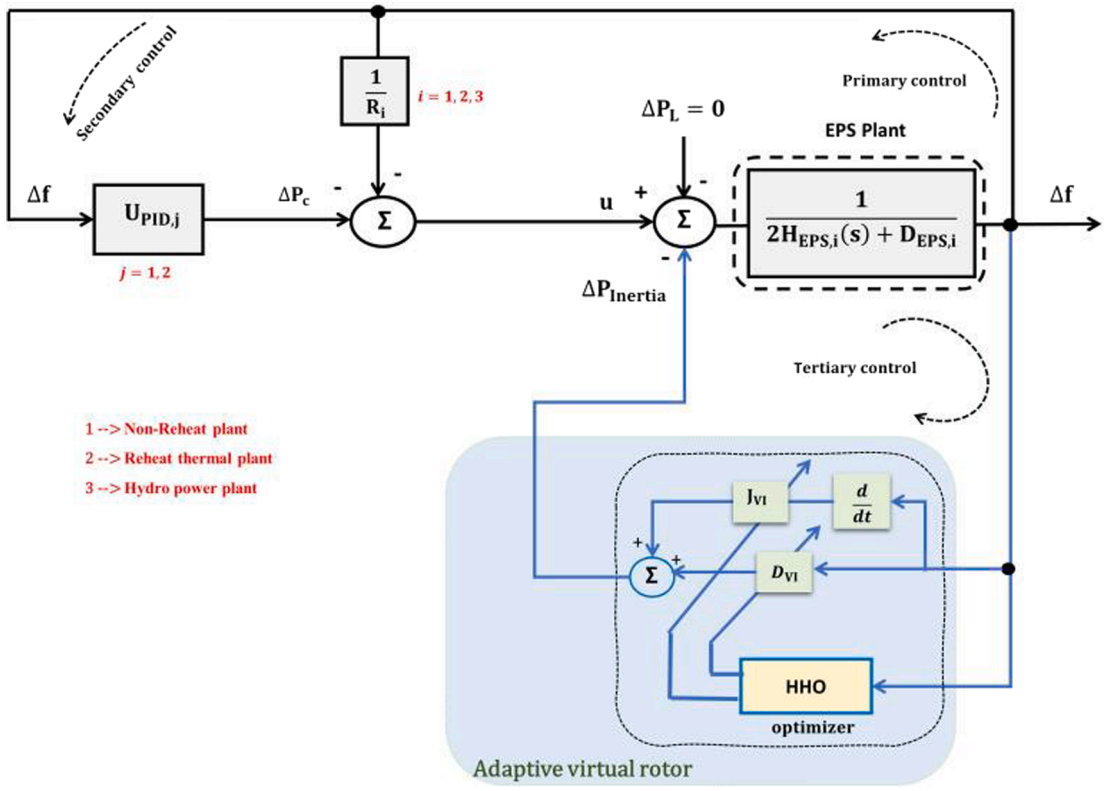

Fig. 6. A simplified EPS model using adaptive modified virtual rotor-based HHO optimizer.

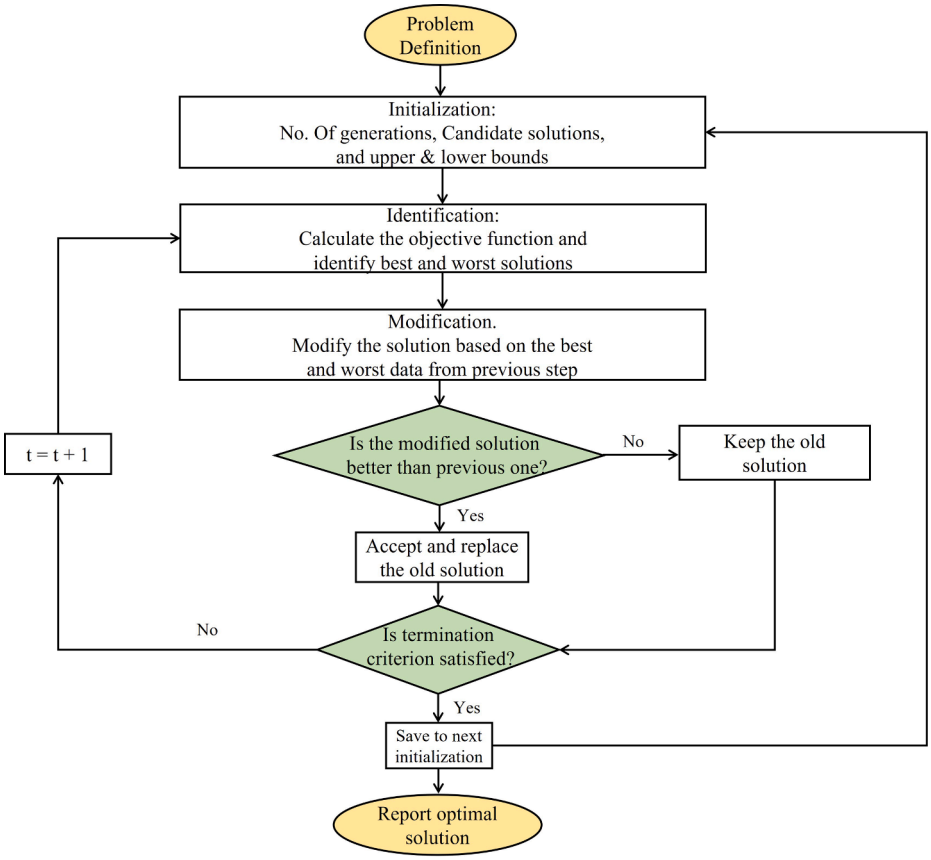

Fig. 7. Overall HHO flowchart with the proposed control strategy.

non-reheat, and hydro plants were discarded to obtain the characteristics of the second-order system such as $\zeta and \omega_n$. Fig. 6 shows a simplified EPS model used to derive the desired J_{min} for primary, secondary, and tertiary control loops with the help of the HHO technique. The closed-loop transfer function for the EPS can be described as follows:

$$T.F = \frac{\omega_n^2}{s^2 + 2\zeta\omega_n s + \omega_n^2} = \frac{\frac{U_{PID}}{2H_{EPS}}}{s^2 + \frac{1}{2H_{EPS}}\left(D_{EPS} + \frac{K_{ir}+1}{R}\right)s + \frac{U_{PID}}{2H_{EPS}}} \quad (15)$$

For minimization, $(sT_{Ess} + 1)$ is added to the virtual loop, then $\omega_n = \sqrt{\frac{U_{PID}}{2H_{EPS}}}$ and $\zeta = \frac{RD_{EPS}+K_{ir}+1}{R\sqrt{8U_{PID}H_{EPS}}}$

$$M_P = e^{\left(\frac{-\pi^*(\zeta)}{\sqrt{(1-(\zeta)^2)}}\right)} = e^{\left(\frac{-\pi^*\left(\frac{RD_{EPS}+K_{ir}+1}{R\sqrt{8U_{PID}H_{EPS}}}\right)}{\sqrt{\left(1-\left(\frac{RD_{EPS}+K_{ir}+1}{R\sqrt{8U_{PID}H_{EPS}}}\right)^2\right)}}\right)} \quad (16)$$

$$T_s = \frac{4}{\omega_n.\zeta} = \left(\frac{16RH_{EPS}}{RD_{EPS} + K_{ir} + 1}\right) \quad (17)$$

The desired $J_{min}-$ based on HHO optimizer is chosen as [5,8]:

$$J_{min} = \sum (T_s + M_P) \quad (18)$$

The HHO optimizer performance when used in an adaptive manner is considered remarkable, powerful, and unaffected by the wide dimension issue. Finally, Fig. 7 shows the overall flowchart including all step procedures for the HHO optimizer.

6. Results and discussions

The suggested direct adaptive control is applied for EPS to tune the modified virtual rotor (inertia + damping) gains. Matlab/Simulink environment is used to examine the proposed control method. The nominal selection parameters for the studied EPS and HHO optimizer are listed in Tabels 1 and 3. To verify the concept of adaptive control for the modified virtual rotor; EPS with the proposed control strategy was tested under the following two scenarios supported with another case study using a 3-area interconnected microgrid system (MG) [38]:

6.1. First Scenario: The effect of step load changes on the EPS system

In this scenario, the performance of the EPS is investigated with the adaptive modified virtual rotor connected to the primary and secondary control loops under the effect of different step load conditions. Step Load Perturbations (SLPs) of 2% and 10 % are applied to the studied EPS by time t = 2 and 40 s respectively. Fig. 8 shows the frequency deviation of the EPS with the control schematics proposed under SLP conditions. It can be seen that the dynamic performance of the EPS with the proposed control strategy (Adaptive modified virtual rotor-based HHO optimizer) is better than the EPS system with/without the classic virtual rotor. Furthermore, the system's response using the proposed coordinated strategy is faster and has less over/undershoot, settling time, and steady-state error than the other ones. Numerical results for the transient specification (i.e., *MOS*, *MUS*, T_s, *Mean*, and *Std*) for the proposed control scheme under variation in loading conditions are stated in Table 4. The findings ensure a robust performance against system uncertainty and disturbance. Finally, the adaptive concept for a modified virtual rotor within the EPS system demonstrates the durability and superiority of the EPS frequency regulation in the event of changing load and system inertia. Fig. 9 shows the output control signal for virtual inertia (J_{VI}) and damping (D_{VI}) parameters using the HHO optimizer after 20 iterations with five candidate solutions for the optimal solution.

Regarding the increase of the emulation of virtual inertia and virtual damping, the inertia power $\Delta P_{inertia}$ from the ESS also increases as shown in Fig. 10. Positive/negative values indicate the charge/discharge power respectively. Thus, it is clear that the ESS controlled by the suggested modified virtual rotor is highly charged/discharged in response to changes in loading conditions.

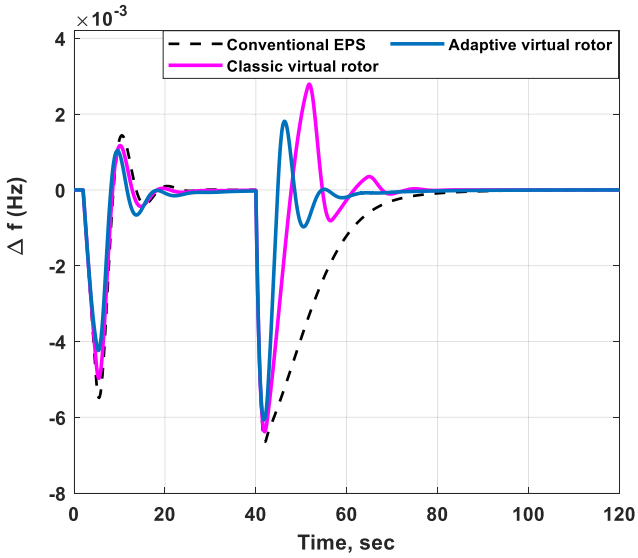

Fig. 8. The EPS frequency deviations due to changes in a) virtual inertia, b) virtual damping.

Table 3
The selection parameters of the HHO algorithm.

Index	Value	
Population size	5	
No. of generations	20	
No. of design variables	2	
Initial value of damping gain (D_{VI})	[1.01,1.33,2.01,2.1,2.28]	Tuned adaptively using HHO optimzer
Initial value of inertia gain (J_{VI})	[5.75,5.21,6.01,6.15,6.5]	

Table 4
The performance specification of the studied EPS system for scenario 1.

SLP %	Parameters	Conventional EPS	Classic virtual rotor	Adaptive virtual rotor
		Δf (Hz)		
2%	*MOS* (pu)	0.001439	0.00117	0.001036
	MUS(pu)	−0.00549	−0.00497	−0.004239
	T_s (s)	20.338	16.4220	14.596
	Std	0.001437	0.00127	0.00107
	Mean	−0.00044	−0.00043	−0.000426
10%	*MOS (pu)*	0.0000	0.00279	0.001812
	MUS(pu)	−0.00665	−0.00638	−0.00607
	T_s *(s)*	86.332	67.2850	57.452
	Std	0.00107	0.00135	0.001070
	Mean	−0.00085	−0.00031	−0.000302

6.2. Second scenario: The effect of the RESs and random loads integrations on the EPS system

The performance of EPS under the integration of RESs and loads on frequency stability concerning the dynamic impacts of power fluctuations produced by PV and load demand is investigated using the adaptive concept for the modified virtual rotor mechanism.

A suggested scenario is performed to demonstrate the effectiveness of the proposed adaptive virtual inertia and virtual damping based HHO

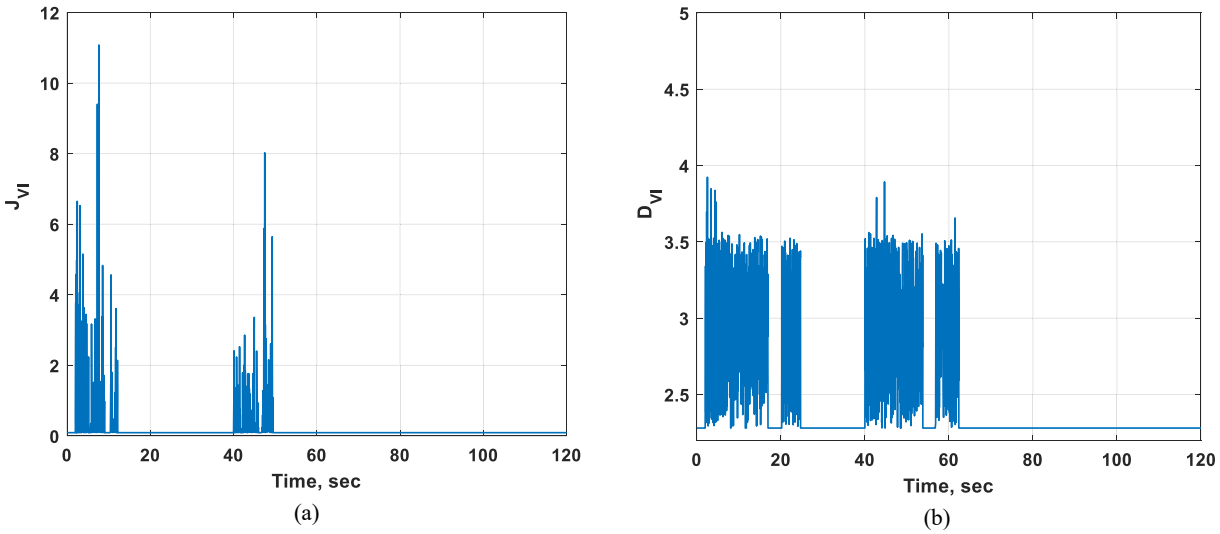

Fig. 9. Output control signal from optimizer for a) virtual inertia, b) virtual damping.

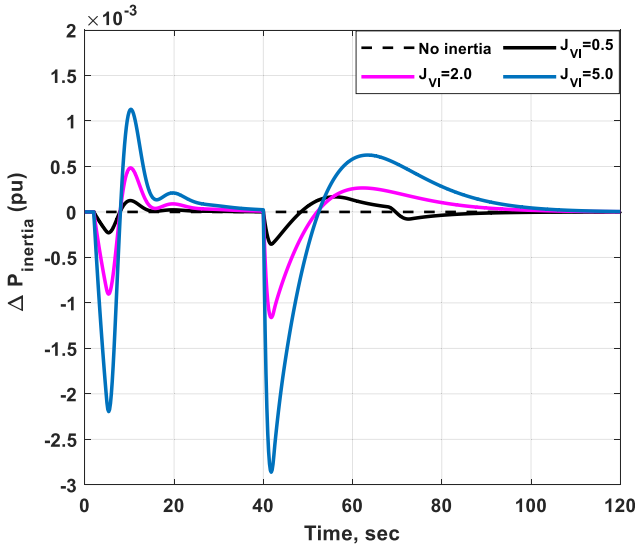

Fig.10. Changes in power inertia for the EPS.

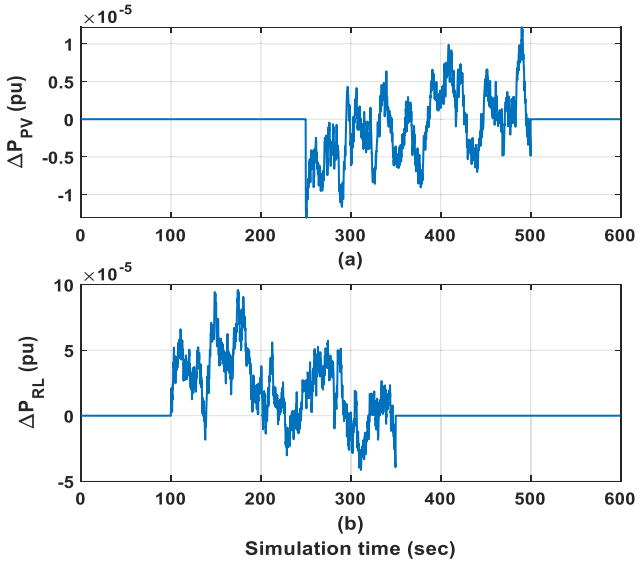

Fig. 11. PV and Load demand power variations.

optimizer compared to the conventional EPS with/without the classic virtual rotor. A partial injection of solar PVs and demand loads are described as: (PV connected to EPS from 250 s and switched off at 500 s, and loads are also connected from 100 s up to 350 s as shown in Fig. 11. Nominal parameters for the modified virtual rotor (inertia + damping) are chosen adaptively using the HHO optimizer within the range mentioned in Table 3. To illustrate the significant impact of RESs penetration on the EPS system, we applied a penetrated PV power generation and load power demand as shown in Fig. 11.

Fig. 12 shows the output control signal of modified virtual rotor parameters using the HHO optimizer with the same nominal selection parameters of scenario 1 for obtaining the optimal solution.

Due to RESs penetration, the system frequency oscillates significantly with higher transient, degraded stability. From Fig. 13, the EPS frequency with the conventional control (primary and secondary) can remain within the standard frequency limit of ± 0.5 Hz as provided by EETC [39], but there are higher fluctuations due to PV/load penetrations at the period of connection /disconnection. This may lead to instability and power outages for the EPS. It is clear that the studied EPS system with the proposed adaptive modified virtual rotor can maintain stability within the desired limit and improve the frequency performance in terms of Max. Over/undershoot, settling time, and steady-state error.

Finally, from Fig. 14, the higher emulation of the modified virtual rotor is also equal to an increase in the inertia power ($\Delta P_{Inertia}$). Therefore, the ESS controlled by the suggested modified virtual rotor is highly charged/discharged in response to any abnormal conditions.

6.3. Case study: Assessment of the proposed direct adaptive concept using multi-area interconnected MG

In this scenario, a 3-area interconnected MG is suggested to examine

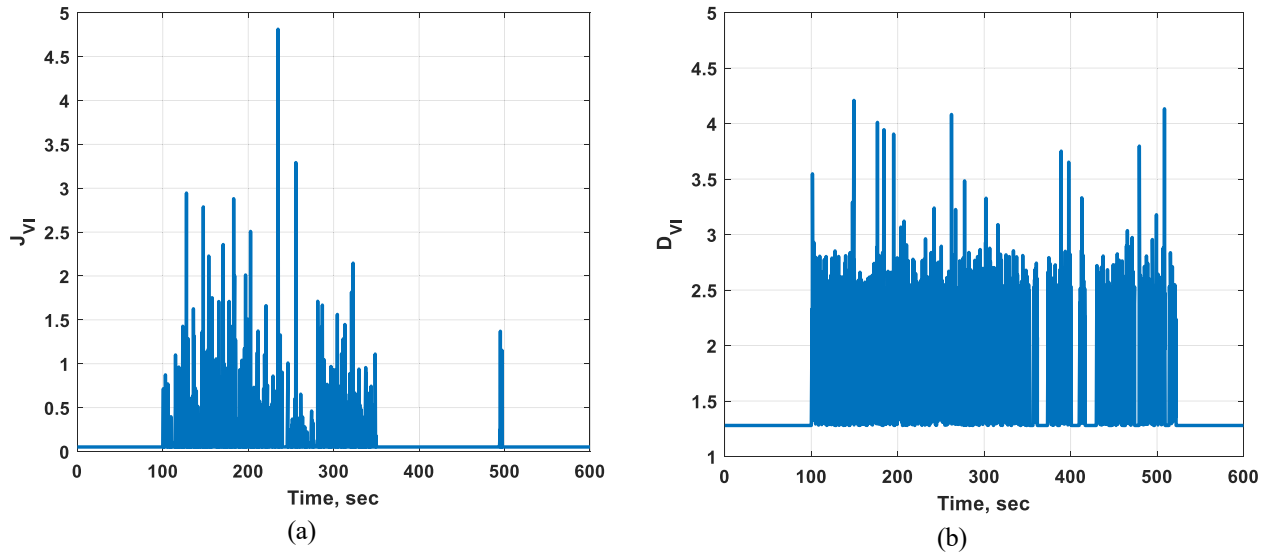

Fig. 12. The output control signal for virtual rotor parameters based HHO for scenario 2: (a) virtual inertia; (b) virtual damping.

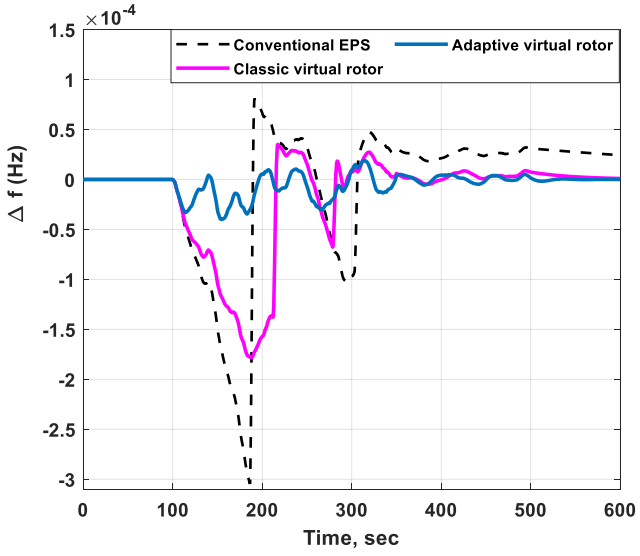

Fig. 13. EPS frequency deviations due to integration of PV and random loads.

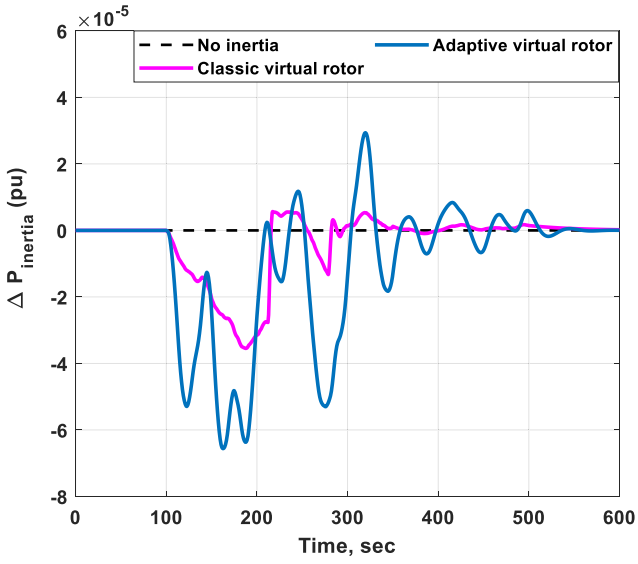

Fig. 14. Changes in power inertia for the EPS with integrated PV and loads.

the efficacy of the proposed direct adaptive control strategy in presence of modified virtual rotor. It is necessary to keep the power of tie-line $\Delta P_{tieline}$ at the scheduled values and to restoring the system frequency to its desired value. Fig. 15 show the simplified model of the 3-area interconnected MG system. The synchronization coefficient between areas are: $T_{12} = 0.2$p.u./rad, $T_{31} = 0.25$p.u./rad and $T_{23} = 0.12$p.u./rad. The full nominal parameters [38] are listed in the Appendix (Table C1).

The system is examined under the effect of a 2.5% change in load ΔP_L at 2 s and the communication time delay is assumed to be 1 s. In Fig. 16, the deviation in frequency for both areas, and the change in tie-line power $\Delta P_{tieline}$ were presented. The system response with the proposed direct adaptive HHO optimizer along with modified virtual rotor improved the overall transient MG performance in terms of (*MOS*, *MUS*, T_s) as compared to conventional MG with/without classic virtual rotor (see Table 5). It is noted from Fig. 16 that the change in tie-line power between both areas and frequency deviation are effectively enhanced with the proposed control strategy compared to other ones.

Finally, from Fig. 17, the higher emulation of the modified virtual rotor is also equal to an increase in the inertia power ($\Delta P_{Inertia}$). Therefore, the ESS controlled by the suggested modified virtual rotor is highly charged/discharged in response to any abnormal conditions.

7. Second application: Single machine connected to the grid

In this research, a dynamic SMIB model considering PSS and AVR is shown in Fig. 18, and a linearized model of an SM tied to the grid is taken as a case study for stability analysis as shown in Fig. 19. The studied system configuration consists of a 200 MVA, 13.8 kV, 50 Hz synchronous generator which is connected to the grid through a 3-phase 13.8/230 kV step-up transformer. In addition, a 10 MW load connected

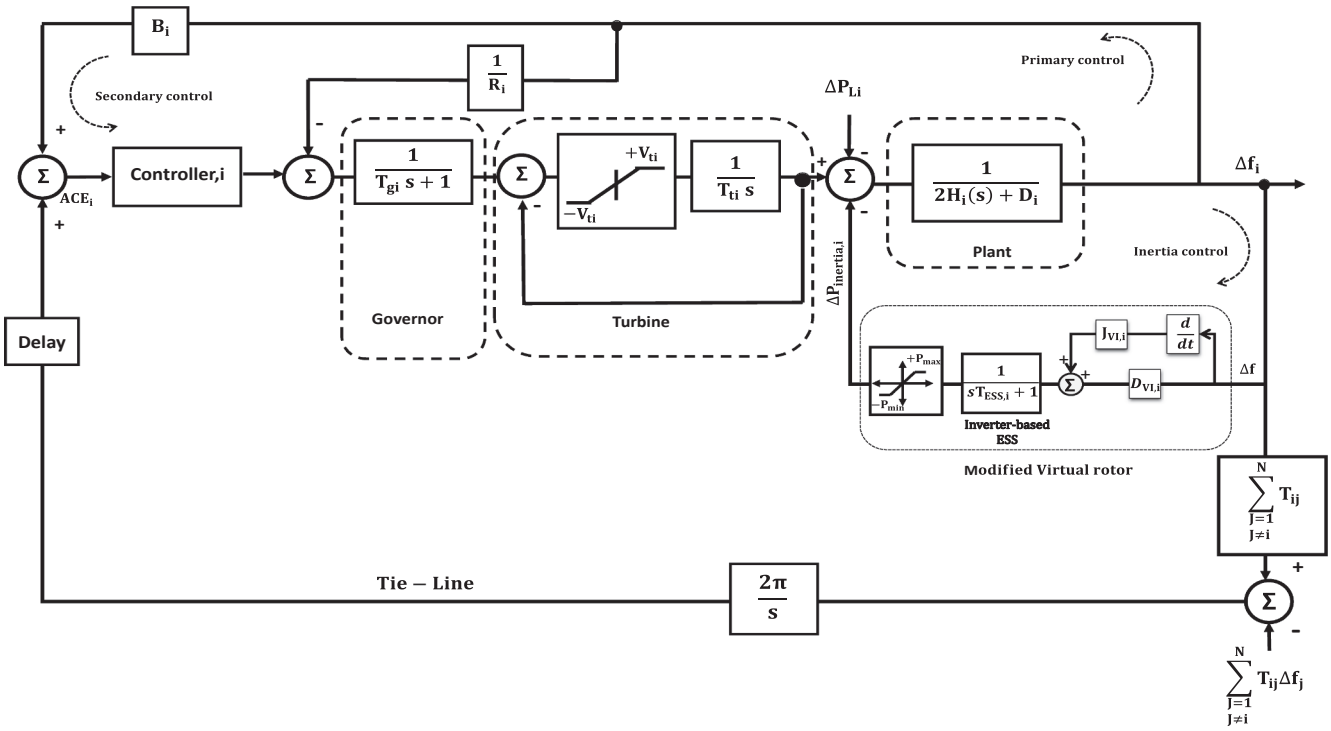

Fig. 15. General model of the multi-area interconnected MG scheme supported by modified virtual rotor.

at the grid side and 25 MW solar PV Farm at the generation side. The synchronous generator is supplied with a hydraulic turbine and governor (HTG), automatic voltage regulator (AVR), and power system stabilizer (PSS). All of the other relevant parameters are listed in Appendix (Table A1).

7.1. Power system stabilizer

The PSS is a device that enriches the performance of dynamic and transient stability of the power system. It acts as an additional supplementary device linked with the AVR or the exciter to develop the stability system constraints [40].

There are several types of PSS devices-based controller such as a standard Lead-Lag PSS, PSS2A based WECC standard method, and PSS2A based PSO (all of them used in this work for comparison only with the proposed adaptive control strategy) [41,42]. Due to its simplicity to implementation and powerful performance, a PID controller is proposed for PSS in this study. The input signal for the PSS stabilizer is represented by the deviation in rotor speed $(\Delta\omega_r)$ as shown in Fig. 20. Additionally, it involves a washout high pass filter which is used to reset the steady-state offset in the PSS output and PSS output boundaries are set to mimic the fluctuation degree of terminal voltage through transient situations. The mathematical representation model of PID, as well as PSS controller, is given as follows [40]:

$$U_{PID} = K_P + \frac{K_i}{s} + K_D.s \tag{19}$$

$$V_{stab} = K_{PSS}\frac{T_{wo}s}{(1+T_{wo}s)}\Delta\omega_r(s) \tag{20}$$

For conventional Lead-Lag PSS, the output actual transfer function $G_p(s)$ can be represent in [41] as:

$$G_p(s) = K_{PSS}\frac{T_{wo}s(1+T_{1o}s)(1+T_{3o}s)}{(1+T_{wo}s)(1+T_{2o}s)(1+T_{4o}s)} \tag{21}$$

Where, K_{PSS} symbolizes stabilizer gain as well as T_{wo} is labeled as the time constant of signal wash out.

$T_{1o} - T_{4o}$ are lead-Lag time constants. K_P, K_i and K_D represent the proportional, integral, and derivative controller gains, respectively which were obtained by the HHO optimizer in offline mode as stated in Appendix (Table A1).

See Fig. 20 for more details about the overall control system and the nominal parameters of the proposed controllers are stated in the Appendix (Table B1).

7.2. Excitation system model

The excitation system of SG provides an excitation voltage E_{fD} to the synchronous machine and regulates its terminal voltage [43]. It plays an important role in the static and dynamic stability of the power system. Fig. 20 shows the configuration of the excitation system based on PID-PSS. It consists of: (i) a low-pass filter, (ii) main regulator, (iii) exciter, (iv) transient gain reduction,, (v) damping filter, and (vi) output limiters.

As mentioned in the previous application for the EPS, the main target is how to calculate the second-order system characteristics ($\zeta and \omega_n$). Therefore, we added a secondary AVR to support the primary AVR within the exciter system. In order to achieve our objective J_{min}, the superposition theorem is used to determine the closed transfer function considering $\Delta\omega_r$ as the main input of the excitation system and neglecting V_2 for simplification as shown in Fig. 21.

For the secondary AVR design, the integral controller gain K_{ir} is

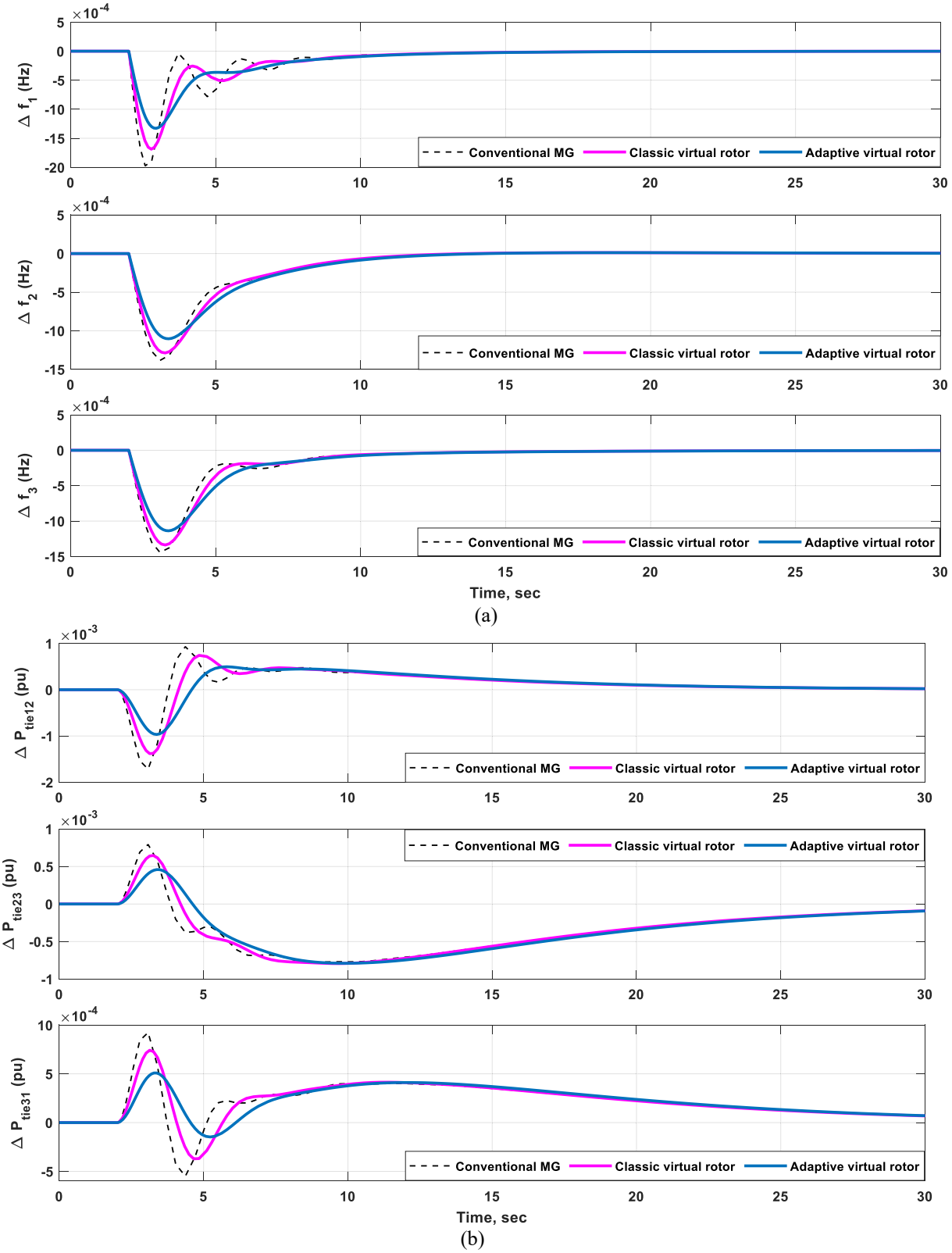

Fig.16. Studied MG system response for 3- area case study: a) frequency deviations b) change in tie-line power.

Table 5
Performance specification of the studied 3-area interconnected MG under the effect of 2.5% load change.

Control area	Parameters	Conventional MG	Classic virtual rotor	Adaptive virtual rotor
		Δf (Hz)		
1	*MOS* (pu)	0.00	0.00	0.00
	MUS(pu)	−0.00198	−0.00169	−0.0013
	T_s (s)	15.821	12.013	10.421
2	*MOS* (pu)	1.11e^{-05}	1.18e^{-05}	1.18e^{-05}
	MUS(pu)	−0.00139	−0.00129	−0.0010
	T_s (s)	14.111	13.508	13.192
3	*MOS* (pu)	0.00	0.00	0.00
	MUS(pu)	−0.00144	−0.00134	−0.0011
	T_s (s)	18.603	12.970	12.407

adaptively tuned using HHO optimizer relying on the speed deviation signal $\Delta\omega_r$ that comes directly from the SG. The time response parameters can be calculated from the second-order feedback system for the proposed adaptive AVR in Fig. 21 as follows:

$$T.F = \frac{\frac{K_E+K_A}{T_AT_E}}{s^2 + \left(\frac{T_AK_E+T_E}{T_AT_E}\right)s + \frac{K_E+K_A}{T_AT_E}} \tag{22}$$

For simplification, S_{fE} is neglected, then

$$\omega_n = \sqrt{\frac{K_E+K_A}{T_AT_E}} \text{and} \zeta = \frac{T_AK_E+T_E}{2T_AT_E\sqrt{\frac{K_E+K_A}{T_AT_E}}}$$

$$M_P = e^{\left(\frac{-\pi*\left(\frac{T_AK_E+T_E}{2T_AT_E\sqrt{\frac{K_E+K_A}{T_AT_E}}}\right)}{\sqrt{\left(1-\left(\frac{T_AK_E+T_E}{2T_AT_E\sqrt{\frac{K_E+K_A}{T_AT_E}}}\right)^2\right)}}\right)} \tag{23}$$

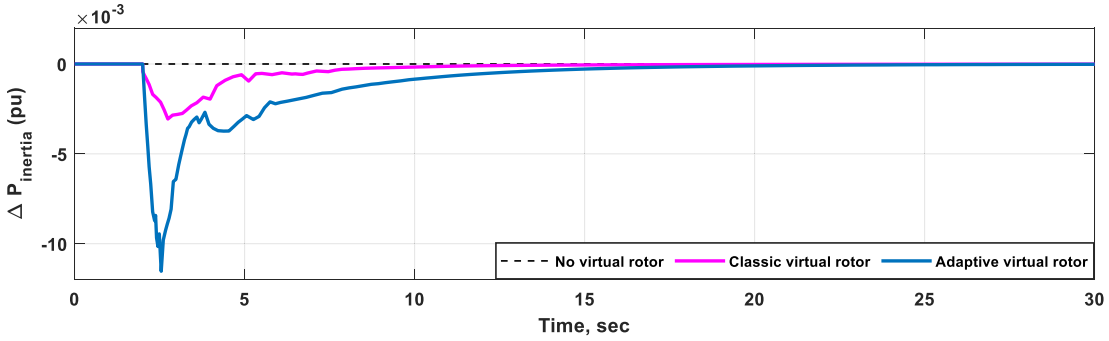

Fig. 17. Changes in power inertia for the studied 3-area interconnected MG.

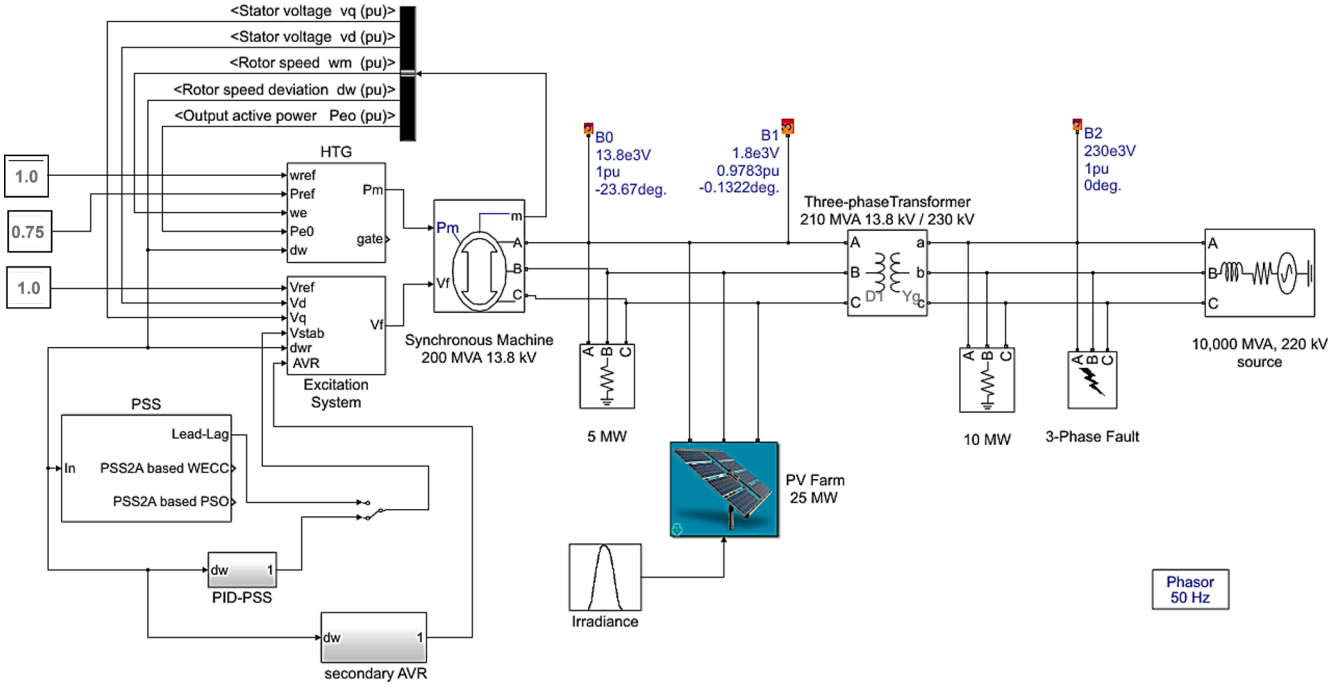

Fig. 18. A simplified Simulink model for SMIB considering PID-PSS and secondary AVR.

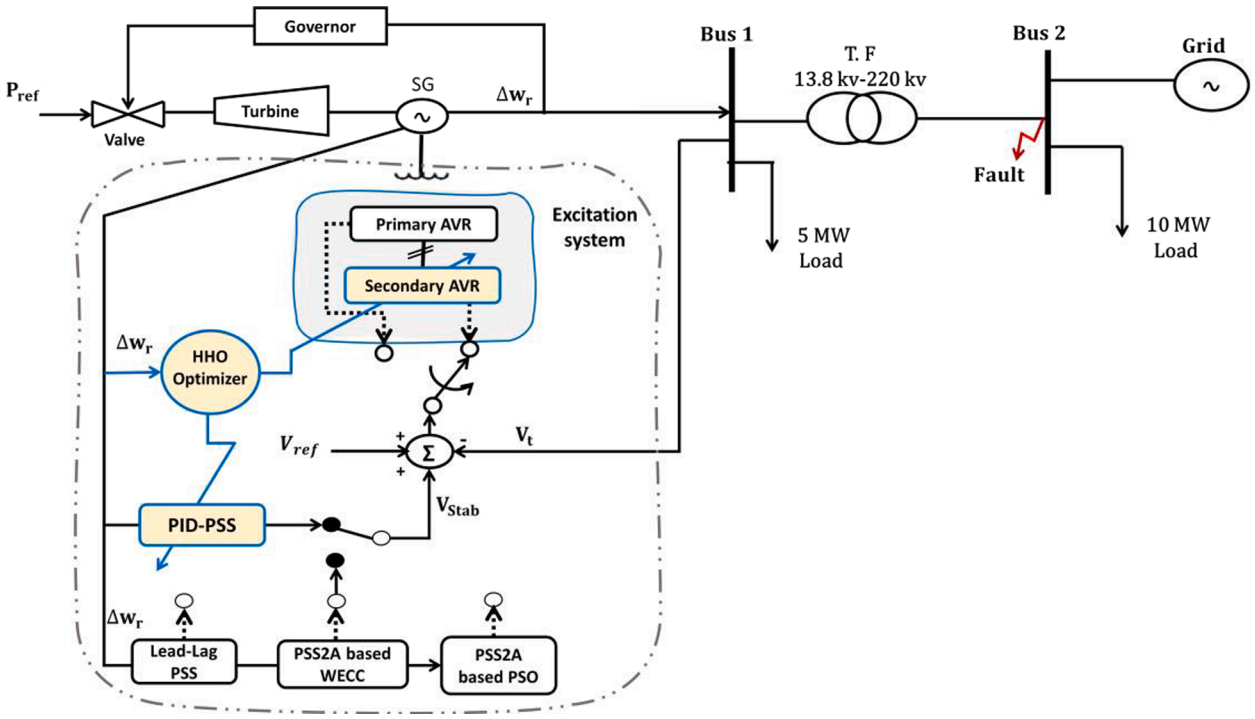

Fig. 19. A linearized model of a single machine connected to an infinite bus with adaptive secondary AVR.

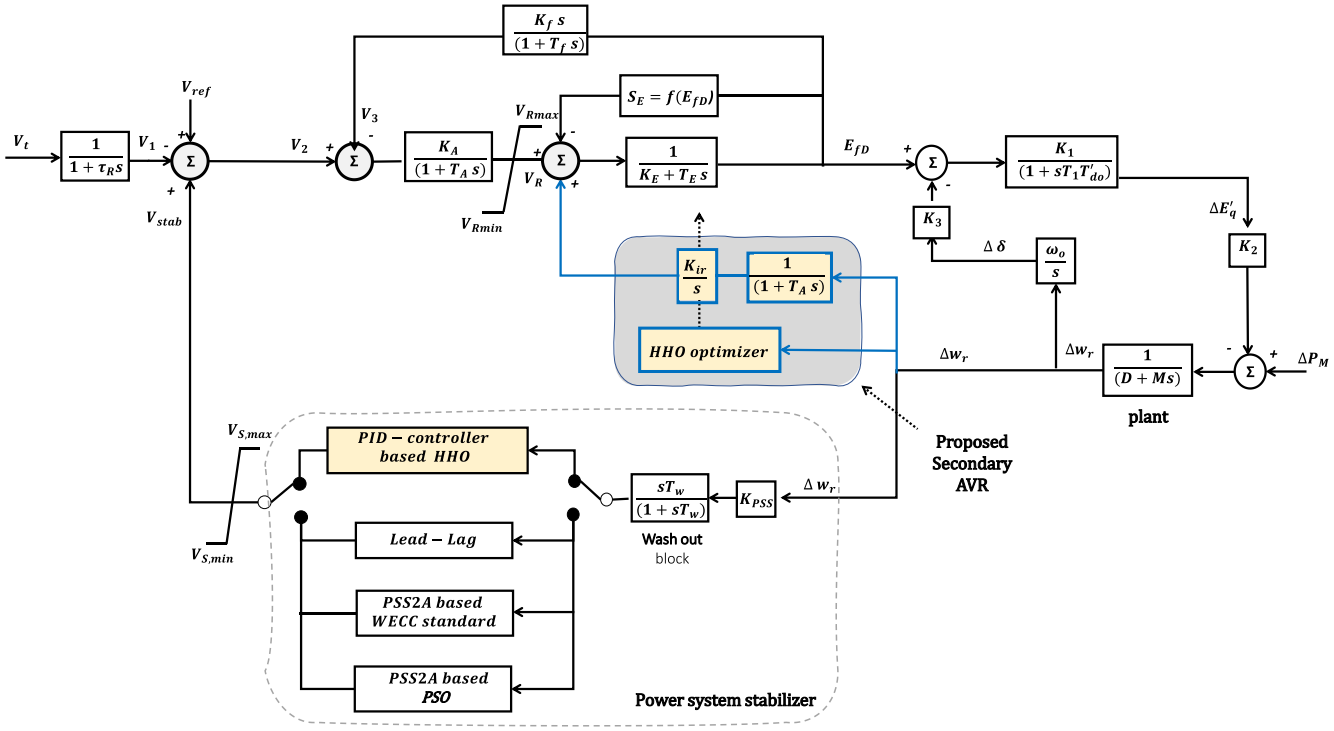

Fig. 20. A complete block diagram of excitation system-based Lead lag, PID-PSS, and proposed secondary AVR.

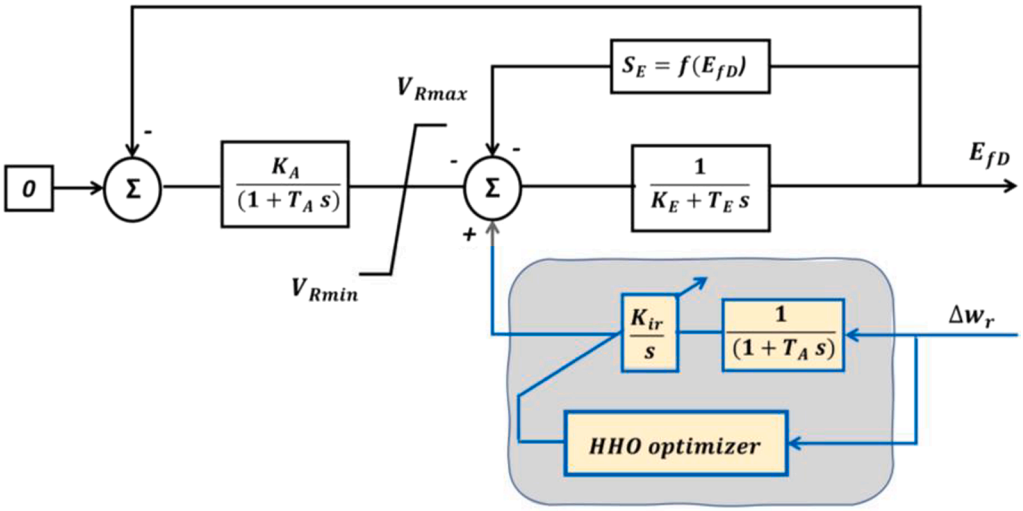

Fig. 21. Simplified block diagram of a closed-loop transfer function for excitation system with the secondary AVR-based adaptive HHO optimizer.

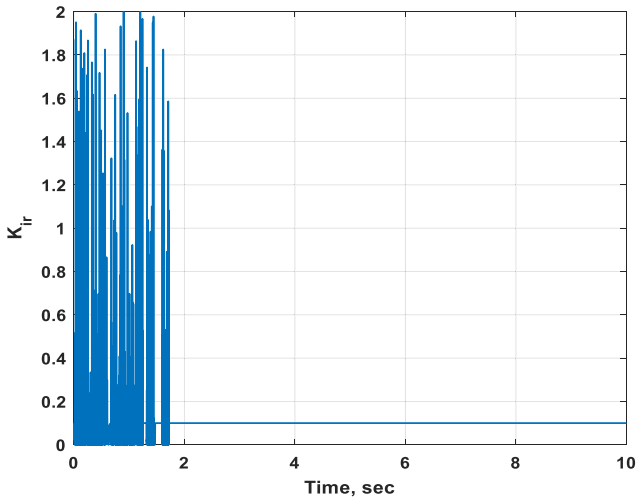

Fig. 22. The integral output control signal for the adaptive secondary AVR-based HHO optimizer.

$$T_s = \frac{8T_A T_E}{(T_A K_E + T_E)} \tag{24}$$

The main objective of PSS and AVR controllers is to enhance the system's response in terms of settling time, overshoot, and undershoot by minimizing the objective function. Therefore, the objective function J_{min} using HHO is suggested as same as Eq. (18).

8. Results and discussions

In this section, the studied single machine system connected to the grid was examined under the effects of a 3ϕ-SC sever fault at the grid bus with/without considering a 25 MW solar PV farm to verify that the proposed adaptive secondary AVR-based HHO optimizer is more excels and accomplished at suppressing oscillations than the conventional SMIB (no PSS) and system with PID-PSS, Lead-lag PSS, PSS2A based WECC standard, and PSS2A based PSO controllers. The performance specifications: (i.e., *MOS*, *MUS*, T_s, and *Std*) has been presented as numerical evidence for the superiority in performance of the proposed direct adaptive control strategy and compared with conventional system, with Lead-Lag PSS, PSS2A based WECC standard, PSS2A based PSO, and PID-PSS controllers. To validate the proposed control strategy, the system was tested in the following two scenario:

8.1. Scenario A: The effect of a three-phase short-circuit fault at the grid bus without PV farm penetrations

In this scenario, the suggested system was examined after applying a 3ϕ-SC fault at the grid bus with disconnection of PV farm as shown in Fig. 18. The fault duration starts from t = 0.1 s until 0.2 s for a simulation time range of 10 s. The purpose is to compare the performance of the conventional system and system with adaptive secondary AVR-based HHO supported by PID-PSS.

Fig. 22 shows the output signal of the integral control gain K_{ir} for the proposed secondary AVR with the same nominal selection parameters used in the first scenario of EPS application to report the optimal solution. Numerical analysis for the proposed (J_{VI}, D_{VI}, K_{ir}) obtained by the applied algorithm are stated in Table 6 using 1 sec as a step size. It is clear from Fig. 23(a)-(e), that the system vibrations are quickly damped when the excitation system is equipped with the proposed secondary AVR adaptively with the help of PID-PSS. In addition, a smooth and modified mechanical power P_M can be obtained using the proposed control technique. The system with the proposed control strategy can afford the best response (lowest settling time and under/overshoot values) as stated in Table 7. Where the deviation in rotor speed ($\Delta\omega_r$) for the conventional system is ± 0.044 rad/s pu and with Lead-Lag, PSS2A based WECC standard, PSS2A based PSO, and PID PSS were kept between ± 0.0132, ±0.0127, ±0.0124, and ± 0.013 rad/s pu respectively. Whereas $\Delta\omega_r$ with the proposed adaptive control strategy was kept between ± 0.009 rad/s pu at the moment of fault event.

Finally, the proposed control strategy (PID-PSS with adaptive secondary AVR-based HHO) provides superior performance in the damping oscillations for the suggested system.

8.2. Scenario B: The effect of a 3ϕ- SC fault at the grid bus considering solar PV farm penetrations

In this scenario, the performance of the studied SMIB using the proposed strategy has been validated in face of a 3ϕ-SC fault at the grid bus considering a 25 MW of solar PV farm as shown in Fig. 18. The main target is to analyze the role of adding the proposed direct adaptive strategy controller in frequency and voltage regulation of renewable-based grid. The fault duration starts from t = 11 s and stays for 0.1 s which assumed to be occurred at the higher irradiance moment (simulated as afternoon).

Fig. 24a–c shows the simulation results of irradiance, power, voltage, and current of the solar PV system. The generation of PV plant varies according to solar irradiance at the moment of fault occurred. Fig. 24d-

Table 6
Output optimizer data analysis for the proposed parameters.

Type of application											
EPS					SMIB	EPS					SMIB
	Scenario 1		Scenario 2				Scenario 1		Scenario 2		
Period (s)	J_{VI}	D_{VI}	$J_{VI} \times 10$	$D_{VI} \times 10$	$K_{ir}/10$	Period (s)	J_{VI}	D_{VI}	$J_{VI} \times 10$	$D_{VI} \times 10$	$K_{ir}/10$
0	0.0912	2.8	0.0515	1.28	0.1	25–40	0.0912	2.28	0.4351	1.636	–
1	0.0912	2.28	0.0515	1.28	0.10975	41	1.2094	2.4661	0.0515	1.28	–
2	0.0912	2.28	0.0515	1.28	0.07787	42	0.0912	2.8231	0.0515	1.28	–
3	0.19363	2.998	0.0515	1.28	0.00134	43	0.20227	3.0198	0.0515	1.3014	–
4	0.65364	3.0606	0.0515	1.28	0.01332	44	0.12006	2.4559	0.0515	1.4691	–
5	0.7365	2.6085	0.0515	1.28	0.01333	45	0.85988	2.8798	0.0515	2.13	–
6	0.22486	3.1577	0.0515	1.28	0.00730	46	0.1719	2.8156	0.0515	1.647	–
7	0.26948	3.1445	0.0515	1.28	$5.204e^{-09}$	47	0.25312	2.6253	0.0515	1.4977	–
8	0.1562	3.3267	0.0515	1.28	0.04744	48	0.22738	3.1395	0.0515	1.5918	–
9	0.77159	2.8866	0.0515	1.28	2.0	49	0.13385	3.2959	0.8228	2.0636	–
10	0.0912	2.9982	0.0515	1.28	0.1	50	0.0912	2.3628	0.0515	2.3112	–
11	0.19439	2.4876	0.0515	1.8684	0.03532	51	0.0912	2.4227	0.0515	1.28	–
12	0.09685	2.5111	0.0515	2.2468	0.00019	52	0.0912	3.0211	0.0515	1.4137	–
13	0.0912	3.337	0.0549	2.2265	0.1	53	0.0912	3.3104	0.0515	1.28	–
14	0.0912	2.9779	0.0515	2.5247	0.01245	54–56	0.0912	2.28	0.0515	1.28	–
15	0.0912	3.0657	0.0515	2.0997	0.1	57	0.0912	3.2812	0.0515	1.28	–
16	0.0912	2.5315	0.0515	2.2591	0.00172	58	0.0912	3.4423	0.0515	1.28	–
17–20	0.0912	2.28	0.0615	2.5259	0.1	59	0.0912	3.0708	0.0515	1.28	–
21	0.0912	2.7709	0.0530	2.3055	–	60	0.0912	3.193	0.0515	1.28	–
22	0.0912	2.5984	0.0885	1.28	–	61	–	–	–	–	–
23	0.0912	2.6337	0.0515	1.5409	–	62	–	–	–	–	–
24	0.0912	2.3904	0.1729	2.01	–	63–120	–	–	–	–	–

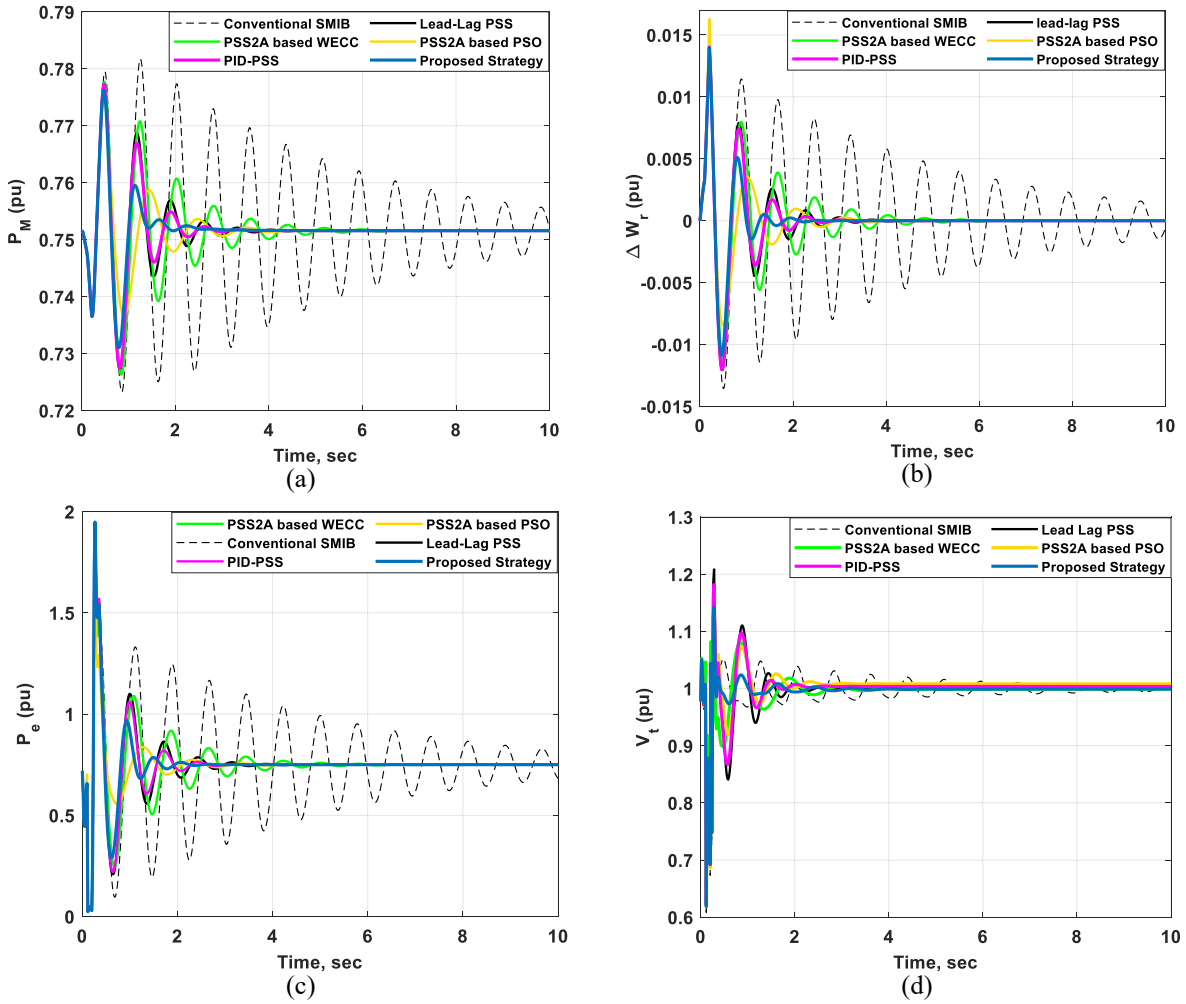

Fig. 23. Transient responses of the studied single machine grid-connected subject to a 3ϕ-SC fault at grid bus (a) P_m; (b) $\Delta\omega_r$; (c) P_e; (d) V_t.

Table 7
Performance Specification Due to a 3ϕ-SC fault at bus 2.

Variable	Index	Conventional system	Lead-Lag PSS	PSS2A based WECC	PSS2A based PSO	PID-PSS	Proposed adaptive control Strategy
$\Delta\omega_r$	*MUS* (pu)	−0.07356	−0.01207	−0.01138	−0.00845	−0.01202	−0.01088
	MOS(pu)	0.01411	0.01401	0.01394	0.01629	0.01403	0.01399
	T_s (s)	> 10 s	2.485	4.825	2.599	1.880	1.099
	Std	0.00471	0.00244	0.00258	0.00210	0.00471	0.00205
P_m	*MUS* (pu)	0.7235	0.7271	0.7263	0.7366	0.7274	0.7311
	MOS(pu)	0.7817	0.7773	0.7777	0.7761	0.7773	0.7742
	T_s (s)	> 10 s	2.380	4.719	2.848	2.851	1.330
	Std	0.01181	0.00551	0.00627	0.0045	0.00529	0.00445
P_e	*MUS* (pu)	0.0227	0.0236	0.0235	0.0262	0.0235	0.0248
	MOS(pu)	1.87	1.933	1.871	1.847	1.935	1.847
	T_s (s)	> 10 s	2.432	3.905	1.798	1.725	1.236
	Std	0.2623	0.1631	0.1614	0.1203	0.1593	0.1251
V_t	*MUS* (pu)	0.6082	0.6358	0.6534	0.6187	0.6226	0.6186
	MOS(pu)	1.136	1.208	1.135	1.174	1.182	1.142
	T_s (s)	7.957	1.722	2.350	1.604	1.480	1.093
	Std	0.03362	0.03758	0.03149	0.03346	0.03621	0.02869

24f show the effect of this abrupt event on grid frequency and power shared by the HTG system and solar PV Farm for voltage and frequency regulation of the grid, respectively.

It is clear from Fig. 24(a)-(e), that the system vibrations are quickly damped when the excitation system is equipped with the proposed secondary AVR adaptively with the help of PID-PSS. Where the $\Delta\omega_r$ at fault moment for the conventional system is ± 0.018 rad/s pu and with Lead-Lag, PSS2A based WECC standard, PSS2A based PSO, and PID PSS were kept between ± 0.0108, ±0.011, ±0.009, and ± 0.0107 rad/s pu respectively. Whereas $\Delta\omega_r$ with the proposed adaptive control strategy was kept between ± 0.009 rad/s pu at the moment of fault event.

As a result, the proposed control strategy provides good evidence for robustness against sudden abrupt events over the other comparative methods by improving the overall transient system performance and regulation in frequency and voltage.

9. Conclusion

This work proposes the concept of direct adaptive control-based soft techniques to tune the gains of traditional controller parameters. The proposed control strategy was applied for two different power system applications: the Egyptian power system (EPS) and automatic voltage regulator (AVR) within the excitation system for a single machine connected to grid.

For EPS, three conventional plants were taken as a case study. A tertiary control loop for a modified virtual rotor to emulate virtual inertia and virtual damping is used to support the droop and secondary controllers inside the EPS system. In this study, the direct adaptive control strategy based HHO was investigated for tuning the modified virtual rotor parameters (inertiaJ_{VI} + damping D_{VI}). A comparative performance study between the proposed direct adaptive control strategy and the conventional EPS system with/without classic virtual rotor is performed under different step load conditions, partial injection of PV, and random loads. In addition, a special case study is performed for frequency regulation to assess the efficacy of the proposed strategy using a 3-area interconnected MG.

For Excitation system: A single machine connected to a grid was considered to study. A secondary AVR is added to support the primary AVR within the excitation system. The implications of using the direct adaptive control concept for secondary AVR-based HHO in presence of PID-PSS parameterized offline by the same optimizer to ensure high robust performance and promote the rapid damping of the studied system connected to the power grid are suggested.

In this study, an adaptive HHO optimizer was investigated directly to adjust the secondary AVR's integral gain K_{ir} in the excitation system. The system is examined and inspected under the effect of a 3ϕ- short circuit fault at the grid bus considering a solar PV farm-based grid. The proposed adaptive control strategy (PID-PSS + adaptive secondary AVR-based HHO) ensures high performance by increasing the dynamic stability and improvement of overall and oscillations damping due to any abnormal conditions.

The final findings demonstrated the efficacy of the proposed direct adaptive control concept in each suggested systems. Additionally, it can handle higher perturbations due to step changes, 3ϕ-SC fault conditions, and RESs integrations.

There are some limitations should be considered for future work that observed from using the classic optimizers as a direct adaptive controller such as:

1. The proposed algorithm is depending only on the rotor speed deviation as a feedback signal, which made the objective function solely as a suggested controller gain value. This decreases the efficiency of the control approach in the face of system disturbances or parameter changes.
2. In general, the proposed algorithm has still been applied to small scale optimization problems (<100 design variables). Additionally, for several applications, we do not actually know which objective functions we wish to optimize since they rely on the behaviour of the running model. Therefore, we gather information about the objective function from past observations and use that knowledge to optimize it.

CRediT authorship contribution statement

Hussein Abubakr: Conceptualization, Software, Validation, Writing – original draft. **Juan C. Vasquez:** Visualization, Writing – review & editing. **Tarek Hassan Mohamed:** Methodology, Formal analysis. **Josep M. Guerrero:** Supervision, Funding acquisition.

Declaration of Competing Interest

The authors declare that they have no known competing financial interests or personal relationships that could have appeared to influence the work reported in this paper.

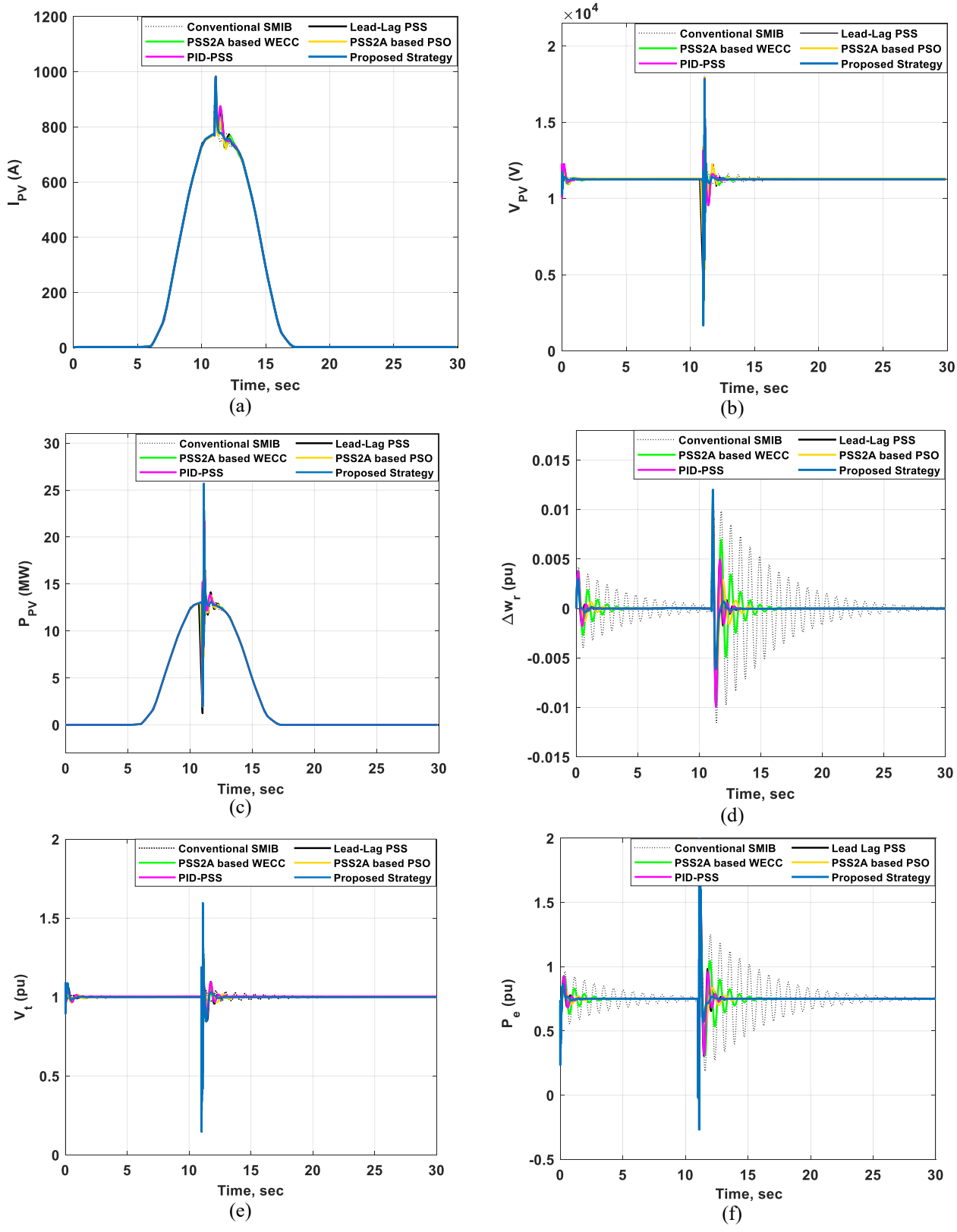

Fig. 24. Transient responses of the studied single machine grid-connected subject to a 3ϕ-SC fault at grid bus considering a solar PV farm: (a) I_{PV}; (b) V_{PV}; (c) P_{PV}; (d) $\Delta\omega_r$; (e) V_t; (f)P_e.

Acknowledgment

Hussein Abubakr is fully funded by the Ministry of Higher Education of the Arab Republic of Egypt; This work is supported by VILLUM FONDEN under the VILLUM Investigator Grant (no. 25920): Center for Research on Microgrids (CROM).

Appendix

Table A1

Table A1
A single machine based synchronous generator connected to grid parameters.

a) Hydro-turbine generator		
Servomotor $[K_a(), T_a(s)]$	[10/3 0.07]	
Gate opening limits $[g_{min}, g_{max}, vg_{min}, vg_{min}(pu/s)]$	[0.01 0.97518–0.1 0.1]	
Permanent droop and regulator $[R_p() K_P() K_I() K_d() T_{wd}(s)]$	[0.05 1.163 0.105 0 0.01]	
Hydraulic turbine [*beta* $() T_w(sec)$]	[0 2.67]	
Initial mechanical power (pu):	0.751606	
b) Synchronous generator		
Nominal power(VA), line-to-line voltage (Kv), and frequency (Hz)	[200e^6, 13.8, 50]	
Stator [R_s] (**pu**)	[0.00285]	
Field [R_f, L_{1fd}] (**pu**)	[0.000579, 0.114]	
Inertia coefficient, friction factor, poles $[H(s) F(pu), p()]$	[3.2, 0, 2].	
d) Three-phase Transformer		
Nominal power and frequency $[P_n(MVA), f_n(Hz)]$	[210, 50]	
Winding 1 parameters $[V_{1Ph-Ph}(rms), R_1(pu), L_1(pu)]$	[13.8e3, 0.0027, 0.08]	
Winding 2 parameters $[V_{2Ph-Ph}(rms), R_2(pu), L_2(pu)]$	[230e3, 0.0027, 0.08].	
Magnetizing resistance $R_m(pu)$	500	
Magnetizing inductance $L_m(pu)$	500	
e) Excitation system		
Low-pass filter time constant $T_r(s)$	0.02	
Regulator gain and time constant $[K_a(), T_a(s)]$	[300, 0.001]	
Exciter gain and time constant $[K_e(), T_e(s)]$	[1, 1e-3]	
Damping filter gain and time constant $[K_f(), T_f(s)]$	[0.001, 0.1]	
Regulator output limits and gain $[E_{Fmin}(), E_{Fmax}, K_p()]$	[-11.5, 11.5, 0].	
c) Local load		
Active power for load 1	5 MW	
Active power for load 2	10 MW	
g) Power system stabilizer		
Stabilizer gain $[K_{PSS}]$	1.0	
Washout time constant $[T_w(s)]$	10	
PID gains $[K_P, K_I, K_D]$	[0.0523, 8.50, 5.01]	These parameters were obtained by HHO optimizer in offline mode

Table B1
Parameters of the standard PSS and PSS2A controllers [41,42].

Type	Method	T_1	T_2	T_3	T_4	T_6	T_7	T_8	T_9	K_p	K_{s1}	K_{s2}	M	$V_{S,min}$	$V_{S,max}$
PSS	Lead-Lag	0.05	3	0.02	5.4	–	–	–	–	30	–	–	–	−0.15	0.15
PSS2A	WECC	0.065	0.05	0.2	0.7	0	6	0.13	0.04	1	8	0.5	5	−0.1	0.1
	PSO	0.74	0.44	0.37	0.025	0	6	0.44	0.57	1	7.19	21.8	5	−0.1	0.1

Table C1
Nominal Parameters of the traditional 3-area interconnected MG [38].

Control area	T_t (s)	T_t (s)	D (pu/Hz)	H (pu.s)	β (pu/Hz)	R (Hz/pu)	α	T_{ij} (pu/rad)
1	0.30	0.10	1.0	5.0	21.0	0.05	1.0	$T_{12} = 0.20$
2	0.40	0.17	1.5	6.0	21.5	0.05	1.0	$T_{23} = 0.12$
3	0.35	0.20	1.8	6.0	21.8	0.05	1.0	$T_{31} = 0.25$

References

[1] Ma M, Zhang C, Liu X, Chen H. Distributed model predictive load frequency control of the multi-area power system after deregulation. IEEE Trans Ind Electron 2016; 27:5129–39.
[2] Tran A-T, Le Ngoc Minh B, Tran PT, Huynh VV, Phan V-D, Pham V-T, et al. Adaptive Integral Second-Order Sliding Mode Control Design for Load Frequency Control of Large-Scale Power System with Communication Delays. Complexity 2021;2021:1–19.
[3] Abubakr H, Mohamed TH, Hussein MM, Guerrero JM, Agundis-Tinajero G. Adaptive frequency regulation strategy in multi-area microgrids including renewable energy and electric vehicles supported by virtual inertia. Int J Electr Power Energy Syst. 2021;129:106814.
[4] Sheble G. Power systems (review of "Robust Power System Frequency Control" by Bevrani, H.; 2009) [Book reviews]. IEEE Power Energy Mag 2009;7(5):77, 79–80.
[5] Mohamed TH, Abubakr H, Alamin MAM, Hassan AM. Modified WCA-based adaptive control approach using balloon effect: electrical systems applications. IEEE Access 2020;8:60877–89.
[6] Vafamand N, Arefi MM, Asemani MH, Dragicevic T. Decentralized Robust Disturbance-Observer based LFC of Interconnected Systems. *IEEE Trans Ind Electron* (Early Access) 2022;69(5):4814–23.
[7] Khan M, Sun H. Complete Provision of MPC based LFC by Electric Vehicles with Inertial and Droop Support from DFIG Wind Farm. *IEEE Trans Power Delivery* (Early Access) 2021.
[8] Dahab YA, Abubakr H, Mohamed TH. Adaptive load frequency control of power systems using electro-search optimization supported by the balloon effect. IEEE Access 2020;8:7408–22.
[9] Naga Sai Kalyan CH, Sambasiva Rao G. Frequency and voltage stabilisation in combined load frequency control and automatic voltage regulation of multiarea system with hybrid generation utilities by AC/DC links. Int J Sustain Energ 2020; 39(10):1009–29.
[10] Barakat M, Donkol A, Hamed HFA, Salama GM. Harris hawks-based optimization algorithm for automatic LFC of the interconnected power system using PD-PI cascade control. J Electr Eng Technol 2021;16(4):1845–65.
[11] Safari A, Babaei F, Farrokhifar M. A load frequency control using a PSO-based ANN for micro-grids in the presence of electric vehicles. Int J Ambient Energy 2021;42 (6):688–700.
[12] Kerdphol T, Rahman FS, Watanabe M, Mitani Y, Turschner D, Beck H-P. Enhanced Virtual Inertia Control Based on Derivative Technique to Emulate Simultaneous Inertia and Damping Properties for Microgrid Frequency Regulation. IEEE Access 2019;7:14422–33.
[13] Beck HP, Hesse R. Virtual synchronous machine. In: Proc. 9th Int. Conf. Elect. Power Qual. Utilisation (EPQU); 2007. p. 1-6.
[14] Driesen J, Visscher K. Virtual synchronous generators. Proc. 21st Century IEEE Power Energy Soc. Gen. Meeting, Convers. Delivery Elect. Energy (PES) 2008.:1–3.
[15] Cheema KM. A comprehensive review of virtual synchronous generator. Int J Electr Power Energy Syst 2020;120:106006. https://doi.org/10.1016/j.ijepes.2020.106006.
[16] Patel P, Patel J, Sidhpuria H. Study of Excitation System and Power System Stabilizer for Single Machine Infinite Bus System. Int J Eng Res Technol (IJERT) 2021;10(6).
[17] Liu H, Su J, Yang Y, Qin Z, Li C. Compatible decentralized control of AVR and PSS for improving power system stability. IEEE Syst J 2021;15(2):2410–9.
[18] Oshnoei A, Sadeghian O, Mohammadi-Ivatloo B, Blaabjerg F, Anvari-Moghaddam A. Data-Driven Coordinated Control of AVR and PSS in Power Systems: A Deep Reinforcement Learning Method. In: In 2021 IEEE International Conference on Environment and Electrical Engineering: EEEIC; 2021. p. 1–6.
[19] Zhang Y, Preece R. A comprehensive methodology for assessing power oscillation damping controllers for HVDC-based system stabilization. In: 2015 IEEE Eindhoven PowerTech, IEEE; 2015. p. 1-6.
[20] Zhang T, Mao C, Zhang J, Tian J, Yu M, Wu K, et al. Design and field application of flexible excitation system damping controllers. IEEE Trans Ind Electron 2021;68 (2):949–59.
[21] Zhang T, Cheng L, He S, Yu M, Mao C, Wang D, et al. Optimal design method of flexible excitation system for improving power system stability. IEEE Trans Ind Appl 2021;57(3):2120–8.
[22] Nahas N, Abouheaf M, Sharaf A, Gueaieb W. A Self-Adjusting Adaptive AVR-LFC Scheme for Synchronous Generators. IEEE Trans Power Syst 2019;34(6):5073–5.
[23] Sahu BK, Pati TK, Nayak JR, Panda S, Kar SK. A novel hybrid LUS–TLBO optimized fuzzy-PID controller for load frequency control of multi-source power system. Int J Electr Power Energy Syst 2016;74:58–69.
[24] Nahas N, Abouheaf M, Darghouth MN, Sharaf A. A multi-objective AVR-LFC optimization scheme for multi-area power systems. Electr Power Syst Res 2021; 200:107467. https://doi.org/10.1016/j.epsr.2021.107467.
[25] Babu NR, Saikia LC, Bhagat SK, Saha A. In: Maiden application of hybrid crow-search algorithm with particle swarm optimization in LFC studies. Singapore: Springer; 2021. p. 427–39.
[26] Bošković MČ, Šekara TB, Rapaić MR. ˇTomislav BS, ˇMilan RR. Novel tuning rules for PIDC and PID load frequency controllers considering robustness and sensitivity to measurement noise. Int J Electr Power Energy Syst 2020;114:105416. https://doi.org/10.1016/j.ijepes.2019.105416.
[27] Gheisarnejad M, Khooban MH. Secondary load frequency control for multi-microgrids: HiL real-time simulation. Soft Comput 2019;23(14):5785–98.
[28] Praptodiyono S, Maghfiroh H, Hermanu C. BLDC Motor Control Optimization Using Optimal Adaptive PI Algorithm. Jurnal Elektronika dan Telekomunikasi 2020;20(2):47–52.
[29] Heidari AA, Mirjalili S, Faris H, Aljarah I, Mafarja M, Chen H. Harris hawks optimization: Algorithm and applications. Future Generation Computer Syst 2019; 97:849–72.
[30] Magdy G, Shabib G, Elbaset AA, Mitani Y. Optimized coordinated control of LFC and SMES to enhance frequency stability of a real multi-source power system considering high renewable energy penetration. Prot Control Mod Power Syst 2018;3(1):1–15.
[31] EEHC. *Annual report 2018/2019*. Egyptian Electricity Holding Company, Egypt; 2019. Available: http://www.moee.gov.eg/english_new/report.aspx.
[32] NREA. *Annual report 2020*. New & Renewable Energy Authority, Cairo, Egypt; 2020. Available: http://nrea.gov.eg/test/en/Media/Reports; [accessed September 2020].
[33] Abubakr H, Guerrero JM, Vasquez JC. Modified Virtual Inertia Mechanism Based ESS for A real Multi-Source Power System Application: the Egyptian Grid. In 47th Annual Conference of the IEEE Industrial Electronics Society (IES), IECON. 2021.
[34] Kundur P. Power System Stability and Control. New York: McGraw-Hill Books; 1994. p. 581.
[35] Kreisselmeier G. A robust indirect adaptive-control approach. Int J Control 1986; 43(1):161–75.
[36] Saxena S, Hote YV. Load frequency control in power systems via internal model control scheme and model-order reduction. IEEE Trans Power Syst 2013;28(3): 2749–57.
[37] Dehuri P, Hote YV. Indirect IMC based PID Controller Design for Single Area LFC System in the Presence of Uncertainty and Communication delay. In: In IEEE Texas Power and Energy Conference (TPEC); 2021. p. 1–6.
[38] ShangGuan X-C, He Y, Zhang C-K, Jin Li, Jiang L, Wu M, et al. Switching system-based load frequency control for multi-area power system resilient to denial-of-service attacks. Control Eng Pract 2021;107:104678. https://doi.org/10.1016/j.conengprac.2020.104678.
[39] EETC. *Transmission Grid Code*. Egyptian Electricity Transmission Company, Cairo, Egypt; 2021. Available: http://www.eetc.net.eg/grid_code.html.
[40] Ray PK, Paital SR, Mohanty A, Eddy FYS, Gooi HB. A robust power system stabilizer for enhancement of stability in power system using adaptive fuzzy sliding mode control. Appl Soft Comput 2018;73:471–81.
[41] Farhad Z, Ibrahim EKE, Tezcan SS, Safi SJ. A robust PID power system stabilizer design of single machine infinite bus system using firefly algorithm. Gazi Univ J Sci 2018;31(1):155–72.
[42] Ruglheck S, Wangdee W. (2016, June). Power system stabilizer tuning comparison for WECC standard-based and PSO-based methods. In: 2016 13th International Conference on Electrical Engineering/Electronics, Computer, Telecommunications and Information Technology (ECTI-CON), IEEE; 2016. p 1-6.
[43] Mohapatra SK, Senapati MK, Dash SK. Coordinated Design of PSS and AVR for Stability Enhancement Using Differential Evolution Algorithm. In: International Conference on Intelligent Computing and Applications. Singapore: Springer; 2021. p. 387–96.